# Unraveling the Discrepancies between Eulerian and Lagrangian Moisture Tracking Models in Monsoon- and Westerlies-dominated Basins of the Tibetan Plateau

Ying Li[1,2,3], Chenghao Wang[4,5], Qiuhong Tang[6], Shibo Yao[7], Bo Sun[8], Hui Peng[1], and Shangbin Xiao[1,2,3]

[1] College of Hydraulic and Environmental Engineering, China Three Gorges University, Yichang, China
[2] Engineering Research Center of Eco-environment in Three Gorges Reservoir Region, Yichang, China
[3] Three Gorges Reservoir Ecosystem Field Scientific Observation and Research Station, China Three Gorges University, Yichang, China
[4] School of Meteorology, University of Oklahoma, Norman, OK, USA
[5] Department of Geography and Environmental Sustainability, University of Oklahoma, Norman, OK, USA
[6] Key Laboratory of Water Cycle and Related Land Surface Processes, Institute of Geographic Sciences and Natural Resources Research, Chinese Academy of Sciences, Beijing, China
[7] China Meteorological Administration Key Laboratory for Climate Prediction Studies, National Climate Center, Beijing, China
[8] Collaborative Innovation Center on Forecast and Evaluation of Meteorological Disasters/Key Laboratory of Meteorological Disasters, Ministry of Education/Joint International Research Laboratory of Climate and Environment Change, Nanjing University of Information Science and Technology, Nanjing, China

*Correspondence to*: Ying Li (ly_hydro@outlook.com) and Shangbin Xiao (shangbinx@163.com)

**Abstract.** Eulerian and Lagrangian numerical moisture tracking models, which are primarily used to quantify moisture contributions from global sources to specific regions, play a crucial role in hydrology and (paleo)climatology studies on the Tibetan Plateau (TP). Despite their widespread applications on the TP, potential discrepancies in their moisture tracking results and their underlying causes remain unexplored. In this study, we compare the most widely used Eulerian and Lagrangian moisture tracking models over the TP, i.e., WAM–2layers and FLEXPART-WaterSip, specifically focusing on an Indian Summer Monsoon (ISM)-dominated basin (Yarlung Zangbo River Basin, YB) and a westerlies-dominated basin (upper Tarim River Basin, UTB). Compared to the bias-corrected FLEXPART-WaterSip, WAM–2layers model generally estimates higher moisture contributions from westerlies-dominated and distant sources but lower contributions from local recycling and nearby sources downwind of the westerlies. These differences become smaller~~discrepancies can be mitigated with higher spatial and temporal~~ ~~by increasing the spatial temporal~~ resolutions of forcing data in WAM–2layers. A notable advantage of WAM–2layers over FLEXPART-WaterSip is its closer alignment of estimated moisture sources with actual evaporation, particularly in source regions with complex land–sea distributions. However, the evaporation biases in FLEXPART-WaterSip can be partly corrected through calibration with actual surface fluxes. For moisture tracking over the TP, we recommend using high-resolution forcing datasets, prioritizing temporal resolution over spatial resolution, ~~with a focus on temporal resolution~~ for WAM–2layers;~~,~~ while for FLEXPART-WaterSip, we suggest applying bias corrections to optimize the filter for precipitation particles and adjust evaporation estimates.

## 1 Introduction

Moisture tracking through numerical models play a pivotal role in advancing our quantitative understanding of the global and regional atmospheric water cycle, and is crucial for a variety of applications in meteorology, hydrology, and climate science (Gimeno et al., 2012; Gimeno et al., 2020). The Tibetan Plateau (TP) region, often referred to as the "Asia water tower",
40  encompasses the world's highest plateau and has been experiencing a rapid retreat of glaciers and permafrost, accompanied by shifts in precipitation patterns and a pronounced warming trend in recent decades (Yao et al., 2018; Yao et al., 2022). Numerous research efforts based on meteorological analyses and climate proxy indicators (e.g., precipitation and ice-core isotopes) have comprehensively investigated the hydrologic cycle in this region (Yao et al., 2013; Yang et al., 2014; Liu et al., 2020b). Recent advancements in numerical moisture tracking models have further facilitated the quantitative diagnosis of
45  moisture source–receptor relationships across the TP region (Chen et al., 2012; Zhang et al., 2017; Li et al., 2022a). In recent years, numerical moisture tracking has been widely used to analyze precipitation and water resource changes over the TP (Li et al., 2019; Ayantobo et al., 2022; Zhang et al., 2023b), interpret the characteristics of TP's climate proxy indicators (Shao et al., 2021; Li et al., 2022b; Wang et al., 2022), and investigate the impacts of TP's climatic conditions on downstream areas (Zhang et al., 2023a).

50

Table 1 summarizes the numerical moisture tracking studies over the TP for the past twenty years; the utilized models can be broadly classified into two categories: Eulerian and Lagrangian models. The Eulerian moisture tracking approach typically employs a fixed spatial grid system and primarily focuses on averaged physical quantities with predefined grid spacings, while Lagrangian models uses a particle tracking approach to infer the movement of moisture through diagnosing source–receptor
55  relationships. Among these models, the Water Accounting Model-2layers (WAM-2layers) and the FLEXible PARTicle dispersion model (FLEXPART) coupled with the "WaterSip" moisture source diagnostic method (FLEXPART-WaterSip) are the most widely use Eulerian and Lagrangian moisture tracking models, respectively. As suggested in Table 1, existing studies mainly used either Eulerian or Lagrangian moisture tracking models driven by very diverse forcing datasets, meanwhile covering various study periods and regions across the TP. This diversity largely hinders the quantitative comparison of
60  moisture tracking results from different models and the attribution of their discrepancies. Nevertheless, two general patterns can be observed through a quantitative comparison of the long-term moisture tracking results in these studies. First, moisture sources tracked by Eulerian models tend to cover a large part of the western Eurasian continent and can stretch southward to the southern Indian Ocean (Zhang et al., 2017; Li et al., 2019; Li et al., 2022a; Zhang et al., 2024). In contrast, moisture sources tracked by Lagrangian models predominantly extend southward (Chen et al., 2012; Sun and Wang, 2014; Chen et al., 2019;
65  Yang et al., 2020), with broader westward extensions observed in the moisture tracking for the westernmost TP and Xinjiang region (Zhou et al., 2019; Liu et al., 2020a; Yao et al., 2020; Hu et al., 2021). Second, areas with higher evaporation rates, such as the ocean surface, in general contribute more moisture compared to surrounding land areas. While the moisture sources simulated by Eulerian models aligns well with the land–sea distribution (Zhang et al., 2017; Li et al., 2019; Li et al., 2022a;

Zhang et al., 2024), this alignment is less pronounced for Lagrangian models (Chen et al., 2012; Sun and Wang, 2014; Chen
70  et al., 2019; Zhou et al., 2019; Liu et al., 2020a; Yang et al., 2020; Yao et al., 2020; Hu et al., 2021). In this context, we speculate that different moisture tracking methods (both Eulerian and Lagrangian ones) may involve certain unrecognized uncertainties or errors when applied to the TP region. This underscores the pressing need for further exploration to examine the discrepancies among these models to better characterize the complex hydrological processes of the TP.

75  **Table 1: A ~~Overview~~non-exhaustive overview of moisture tracking studies with Eulerian and Lagrangian models in the TP and its vicinity. ~~Note that extensive studies on water isotopes in the TP with moisture tracking simulations are not included here.~~ "E and P" means the model diagnoses evaporation and precipitation separately, while "E—P" means the model diagnoses contributions through water budget (i.e., evaporation minus precipitation).**

|  | Model | Moisture source diagnosis | Study area | Forcing dataset | Study period | Reference |
|---|---|---|---|---|---|---|
| Eulerian | WAM-1layer | E and P | Central-western TP | ERA-I, NCEP-2 | 1979–2013 | Zhang et al. (2017) |
|  | WAM-2layers | E and P | Endorheic TP | ERA-I, MERRA-2, JRA-55 | 1979–2015 | Li et al. (2019) |
|  | WAM-2layers | E and P | Southern/northern TP | ERA-I | 1979–2016 | Zhang et al. (2019a) |
|  | WAM-2layers | E and P | TP | ERA-I | 1979–2015 | Guo et al. (2019) |
|  | WAM-2layers | E and P | TP | ERA-I | 1998–2018 | Zhang (2020) |
|  | WAM-2layers | E and P | TP | ERA-I, MetUM | 1982–2012 | Guo et al. (2020) |
|  | WAM-2layers | E and P | Major basins in TP | ERA-I, MERRA-2, JRA-55 | 1979–2015 | Li et al. (2022a) |
|  | WAM-2layers | E and P | TP (forward tracking oceanic evaporation) | ERA-I, MERRA-2, JRA-55 | 1979–2015 | Li et al. (2022b) |
|  | WAM-2layers | E and P | TP (forward tracking TP evaporation) | ERA5 | 2000–2020 | Zhang et al. (2023a) |
|  | WAM-2layers | E and P | Five typical cells in the TP | ERA5 | 2011–2020 | Zhang et al. (2024) |
|  | CAM5.1 with a tagging method | E and P | Southern/northern TP | MERRA | 1982–2014 | Pan et al. (2018) |
| Lagrangian | FLEXPART | E—P | TP | NCEP-GFS | 2005–2009 (summer) | Chen et al. (2012) |
|  | FLEXPART | Areal source–receptor attribution | Grassland on eastern TP | NCEP-CFSR | 2000–2009 | Sun and Wang (2014) |
|  | FLEXPART | WaterSip | Four regions within TP | ERA-I | 1979–2018 (May–August) | Chen et al. (2019) |
|  | FLEXPART | Areal source–receptor attribution | Xinjiang | NCEP-FNL | 2008–2015 (April–September) | Zhou et al. (2019) |
|  | FLEXPART | WaterSip | Southeastern TP | ERA-I | 1980–2016 (June–September) | Yang et al. (2020) |
|  | FLEXPART | WaterSip | Xinjiang | NCEP-CFSR | 1979–2018 | Yao et al. (2020) |
|  | FLEXPART | WaterSip | Northern/Southern Xinjiang | NCEP-CFSR | 1979–2018 | Hu et al. (2021) |
|  | FLEXPART | Areal source–receptor attribution | Source region of Yellow River | NCEP-FNL | 1979–2009 | Liu et al. (2021) |
|  | FLEXPART | WaterSip | Xinjiang | NCEP-CFSR | 1979–2018 (April–September) | Yao et al. (2021) |
|  | FLEXPART | E—P | Three-rivers headwater region | ERA-I | 1980–2017 (boreal summer) | Zhao et al. (2021) |
|  | FLEXPART | E—P | Three-rivers source region | NCEP-FNL | 1989–2019 | Liu et al. (2022) |
|  | FLEXPART | WaterSip | Three-rivers headwater region | ERA-I | 1980–2017 | Zhao et al. (2023) |

| | | | | | |
|---|---|---|---|---|---|
| HYSPLIT | WaterSip | Three-rivers headwater region | NNR1 | 1960–2017 (June–September) | Zhang et al. (2019b) |
| HYSPLIT | E—P | Western TP | ERA-I | 1979–2018 (winter) | Liu et al. (2020a) |
| HYSPLIT | Maximum specific humidity | Seven regions within TP | NCEP/NCAR | 1961–2015 (summer extreme event) | Ma et al. (2020) |
| HYSPLIT | Contribution function and weighting | TP | NCEP-GDAS | 1950–2015 (extreme precipitation events) | Ayantobo et al. (2022) |
| HYSPLIT | WaterSip | Southern Xinjiang | ERA5 | 2021(June 15–17) | Chen et al. (2022) |
| LAGRANTO | WaterSip | Southeastern TP | ERA-I | 1979–2016 (winter extreme precipitation) | Huang et al. (2018) |
| LAGRANTO | WaterSip | Three regions within TP | ERA-I | 1979–2016 (winter extreme precipitation) | Qiu et al. (2019) |
| LAGRANTO | WaterSip | Northern TP | ERA-I | 2010–2018 (monsoon season) | Wang et al. (2023) |
| QIBT | E and P | Southeastern TP | ERA-I | 1982–2011 (April–September) | Xu and Gao (2019) |

80    It is noteworthy that several studies have employed both Eulerian and Lagrangian models to diagnose moisture sources and perform comparative analyses in other regions. For example, a comparison among RCM-tag (coupled with MM5), WAM, and 3D-T (a modification of QIBT) models in West Africa revealed that the number of vertical layers and the mixing assumption for evaporation significantly influence simulations, especially in regions with strong wind shear (van der Ent et al., 2013). Another comparison between Eulerian and Lagrangian approaches (implemented in the COSMO model) in Europe found that

85    the linkage of moisture uptakes in the atmospheric boundary layer to evaporation in the Lagrangian approach is mostly consistent with the advanced Eulerian model (Winschall et al., 2014). Tuinenburg and Staal (2020) compared a set of moisture tracking models for 7 source locations globally and concluded that the three-dimensional Lagrangian models were most accurate and suitable for areas with relatively complex terrain, as they can better track moisture with strong vertical variability in horizontal transport. Using the Eulerian WRF-WVT model as a benchmark for moisture tracking over the Mediterranean

90    region, Cloux et al. (2021) considered the Lagrangian FLEXPART-WRF model more appropriate for a qualitative description of moisture origin rather than a precise estimation of source contributions. These comparative studies emphasize that the most suitable moisture tracking model depends on the specific case, including but not limited to the research question, spatial extent, and computing resource available. Despite these existing efforts, it remains unclear whether their conclusions are applicable to moisture tracking over the TP, especially concerning the most widely used models in the region. Moreover, the studies on

95    the generation mechanisms of model uncertainties through moisture tracking intercomparison is still lacking.

The overall objective of this study is to investigate potential errors/uncertainties in numerical moisture tracking models and the underlying mechanisms of their discrepancies over the TP. This is achieved through a comparison between the most commonly used Eulerian and Lagrangian models in the region, specifically WAM-2layers and FLEXPART-WaterSip. Given

100   that the TP's climate is mainly influenced by the interactions between the Indian Summer Monsoon (ISM) and mid-latitude westerlies, we selected two representative basins for our comparative analysis: the ISM-dominated Yarlung Zangbo River Basin (YB) and the westerlies-dominated upper Tarim River Basin (UTB) (Fig. S1 in the Supplement). Section 2 describes the mechanisms, forcing data, and numerical settings for both moisture tracking models. Section 3 provides a comprehensive

comparison of the moisture tracking results for both basins. Section 4 delves into the intermediate processes of moisture
tracking in the two models: moisture fluxes in WAM‒2layers and particle trajectories in FLEXPART. To further illustrate the
differences between these two models, Section 5 examines the relationship between the simulated moisture contributions and
actual evaporation from various source regions. Section 6 introduces a two-step bias correction method for FLEXPART-
WaterSip simulations based on a comparison between actual and simulated surface fluxes. Section 7 further investigates the
potential determinants of the observed discrepancies between the two approaches through a series of carefully designed
numerical experiments.

## 2 Eulerian and Lagrangian approaches for moisture tracking: WAM‒2layers and FLEXPART-WaterSip models

In this study, the WAM‒2layers V3.0.0b5 is adopted for Eulerian moisture tracking. This two-layers version, designed to deal
with wind shear in the upper air, is an update to the earlier single-layer version (van der Ent et al., 2010). As illustrated in the
conceptual diagram (Fig. 1a), the underlying principle of WAM‒2layers is the water balance equation (van der Ent et al., 2014),
which in the lower layer is given by:

$$\frac{\partial S_{g,lower}}{\partial t} = -\frac{\partial (S_{g,lower}u)}{\partial x} - \frac{\partial (S_{g,lower}v)}{\partial y} + E_g - P_g \pm F_{v,g} \tag{1}$$

where subscript $g$ denotes the tagged moisture; $S$ is the moisture content in the atmosphere; $t$ is time; $u$ and $v$ are the zonal ($x$)
and meridional ($y$) wind fields, respectively; $E$ is evaporation (which only occurs in the bottom layer); $P$ is precipitation; and
$F_v$ is the vertical moisture transport between the two layers. The model prescribes a two-layer structure, typically dividing at
approximately 810 hPa with a standard surface pressure. Modifications to $F_v$ ($4F_v$ in the net flux direction and $3F_v$ in the
opposite direction) are implemented to account for turbulent moisture exchange. Note that the division between two layers
varies with topography, which decreases to ~520 hPa over the TP (~4000 m).
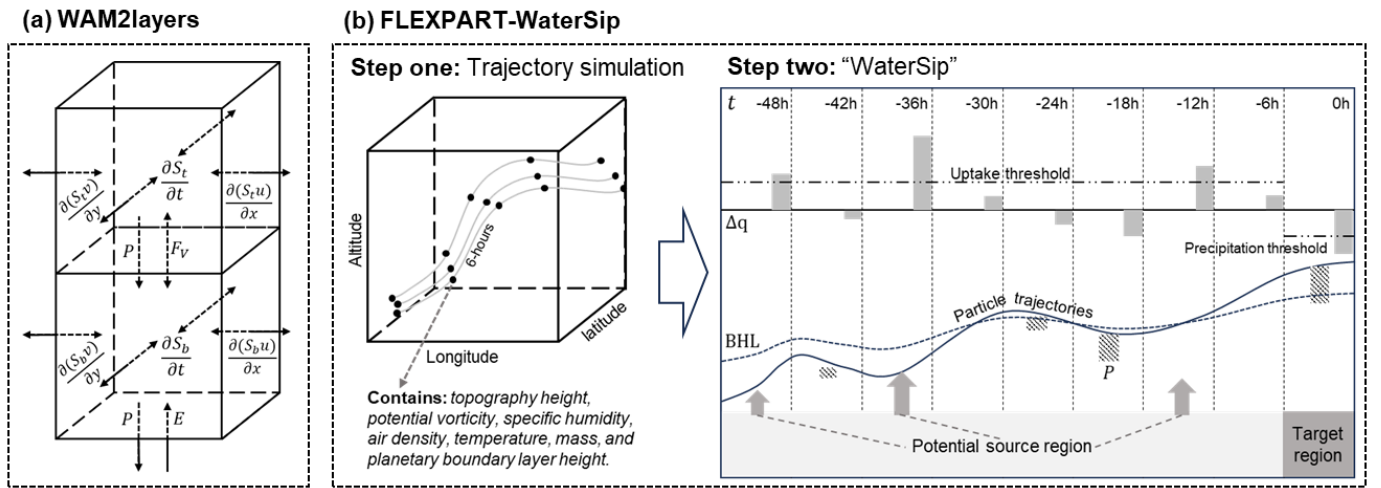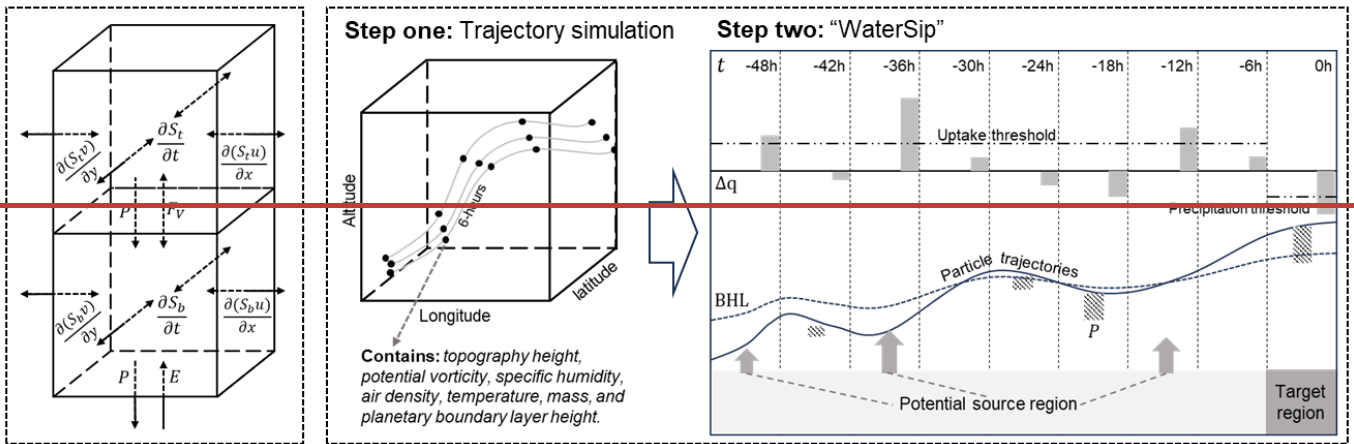
Figure 1: Mechanisms of (a) WAM-2layers and (b) FLEXPART-WaterSip models. "Step two" in (b) is adapted from Sodemann et al. (2008).

The Lagrangian particle trajectory simulation in this study is conducted using FLEXPART V10.4, a versatile model widely employed to simulate the transport and turbulent mixing of gases and aerosols in the atmosphere (Pisso et al., 2019). FLEXPART can operates in domain-filling mode to represent the entire atmosphere using uniformly distributed particles with equal mass. It is independent of a computational grid, which enables effective descriptions of atmospheric transport at a theoretically infinitesimal spatial resolution. For this study, five million particles were released across the entire tracking domain~~at altitudes ranging from 100 m to 20,000 m across the entire target region~~. The outputs from FLEXPART include detailed three-dimensional position, topography height, potential vorticity, specific humidity, air density, temperature, mass, and planetary boundary layer height (BLH) of each particle/parcel at 6-hourly intervals (Fig. 1b). Similar to other

Lagrangian models such as HYSPLIT (Stein et al., 2016) and Lagranto (Sprenger and Wernli, 2015), FLEXPART on its own does not identify potential moisture sources for precipitation in the target region nor quantify their contributions. To address this limitation, we adopted the "WaterSip" method proposed by Sodemann et al. (2008). This method identifiesy moisture sources using humidity information along particle trajectories simulated by FLEXPART, which involves key processes such as filtering trajectories that lead to precipitation, calculating specific humidity changes and their attributed fractions, and determining potential moisture sources based on moisture uptake thresholds and BLH (Fig. 1b). A more detailed description of this method can be found in Sodemann et al. (2008). Default screening thresholds in this study are set at 0.2 g kg$^{-1}$ for specific humidity change, 80% for relative humidity, and 1.5 times the BLH for particle height, although adjustments were made for sensitivity experiments detailed in Sections 6 and 7. In summary, the FLEXPART-WaterSip approach adopted here integrates the particle trajectory simulated by FLEXPART with the moisture source–receptor diagnostics of WaterSip.

Both WAM–2layers and FLEXPART-WaterSip operate as offline models that rely on meteorological fields as forcing inputs. Here we used the fifth-generation atmospheric reanalysis product from the European Centre for Medium-Range Weather Forecasts (ERA5) as the forcing dataset, which benefits from decades of advancements in data assimilation, core dynamics, and model physics (Hersbach et al., 2020). The moisture tracking simulations specifically target July 2022, a month significantly influenced by the ISM in the TP region (Yao et al., 2013; Curio and Scherer, 2016). The moisture tracking domain spans from 30°S to 80°N and from 40°W to 140°E, covering nearly all potential oceanic and terrestrial source regions of precipitation over TP (Chen et al., 2012; Li et al., 2022a). In the simulations, the two representative basins are represented with gridded boundaries as shown in Fig. S1 in the Supplement. Considering the number of particles released, data size, and computational resources needed, both models are driven by 1°×1° and 3-hourly ERA5 data, although some specific variables used in the two models are different due to their distinct physical mechanisms.

In WAM–2layers, tagged moisture is continuously released into Eulerian grids and tracked as it progressively accumulates and diffuses across grids over time. The tagged moisture was released throughout the entire July (from 31-July to 1-July in backward mode), with the backward tracking period extending back to 1 June. A previous study in the TP region demonstrated that a ~30-day tracking period can ensure that approximately 95% of the tagged moisture returns to the ground (Zhang et al., 2017), which is consistent with our numerical experiments in the YB and UTB (Fig. 2a). In comparison, FLEXPART-WaterSip model tracks atmospheric particles released at each step independently, thereby avoiding interference between particles released at different times. This differs from WAM–2layers, which ensures that in FLEXPART-WaterSip moisture released at various times does not converge into the same set of Eulerian grids. Typically, the average residence time of moisture in the atmosphere (~10 days) is used as the tracking period for a single particle release in FLEXPART-WaterSip. To align the tracking duration and maximize the tracking of tagged moisture in both models (Fig. 2), the backward tracking time in FLEXPART-WaterSip was extended to 30 days. For FLEXPART-WaterSip, although large deviations in actual air parcel movements may occur beyond the average 10-day residence time, the associated uncertainties in trajectories beyond this period are unlikely to

170   substantially impact the results, as the majority of moisture uptake occurs within the first 10 days (Sodemann et al., 2008). Our numerical experiments, as illustrated in Fig. 2b, indicate that within the first 10 days (20 days), we traced 89% (99%) of the precipitation moisture in the YB and 97% (99%) in the UTB. Detailed configurations of WAM–2layers and FLEXPART models can be found in Part 2 of the Supplement. ~~The WaterSip source code we developed in this study can be found in Part 3 of the Supplement.~~

175
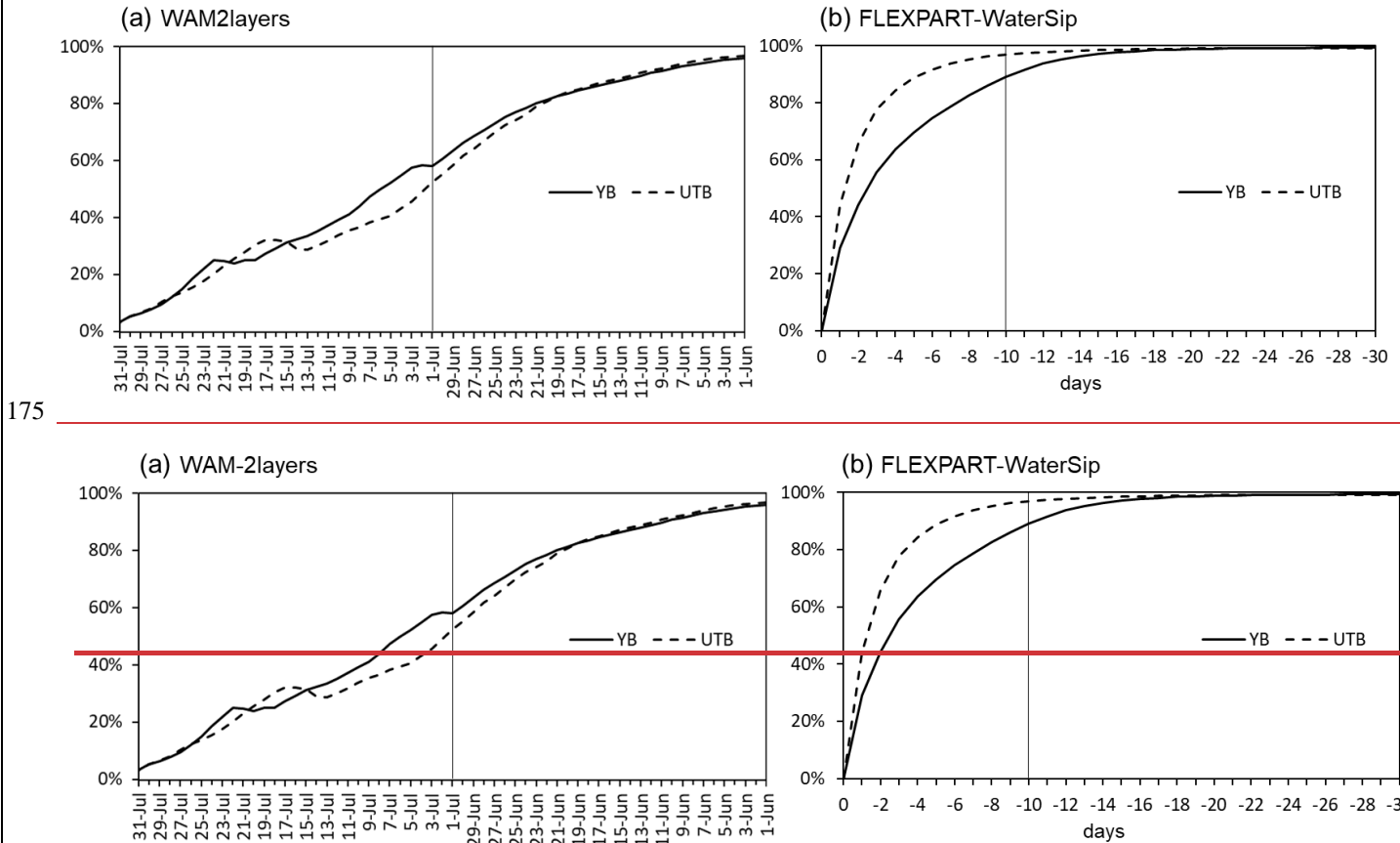
Figure 2. Backward moisture tracking periods and accumulated moisture uptake from all source regions in (a) WAM-2layers and (b) FLEXPART-WaterSip models. Solid lines represent the YB, and dotted lines represent the UTB.

**3 Moisture tracking in two representative basins**

180   Figure 3 shows the simulated moisture sources for precipitation in July 2022 over the YB and UTB based on WAM–2layers and FLEXPART-WaterSip models. Moisture contributions are quantified as equivalent water height (mm) over the source regions. For the YB, in addition to significant local recycling, the distribution of most moisture sources aligns with the path of the ISM, extending from the southern slopes of the Himalayas through the Bay of Bengal (BB) and the Indian subcontinent to

the Arabian Sea (AS), and reaching as far as the Southern Indian Ocean (SIO) (Fig. 3a and c). Moisture sources for the UTB mainly stretch along the westerlies to the Central Asia region (Fig. 3b and d). Generally, WAM–2layers simulations suggest a broader range of distant moisture sources (including both the westerlies-dominated and ISM-dominated regions) when compared to those identified by FLEXPART-WaterSip.

185
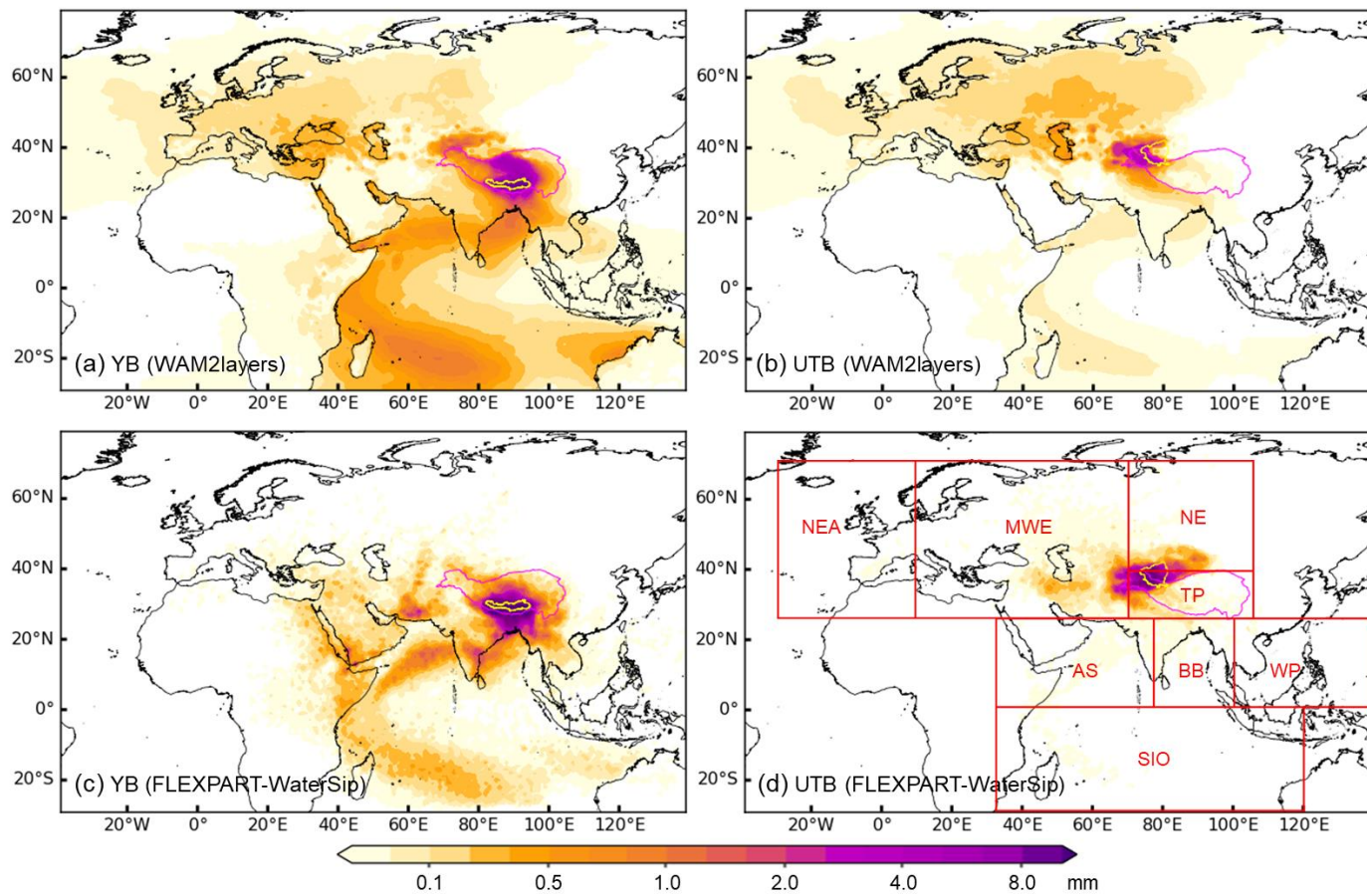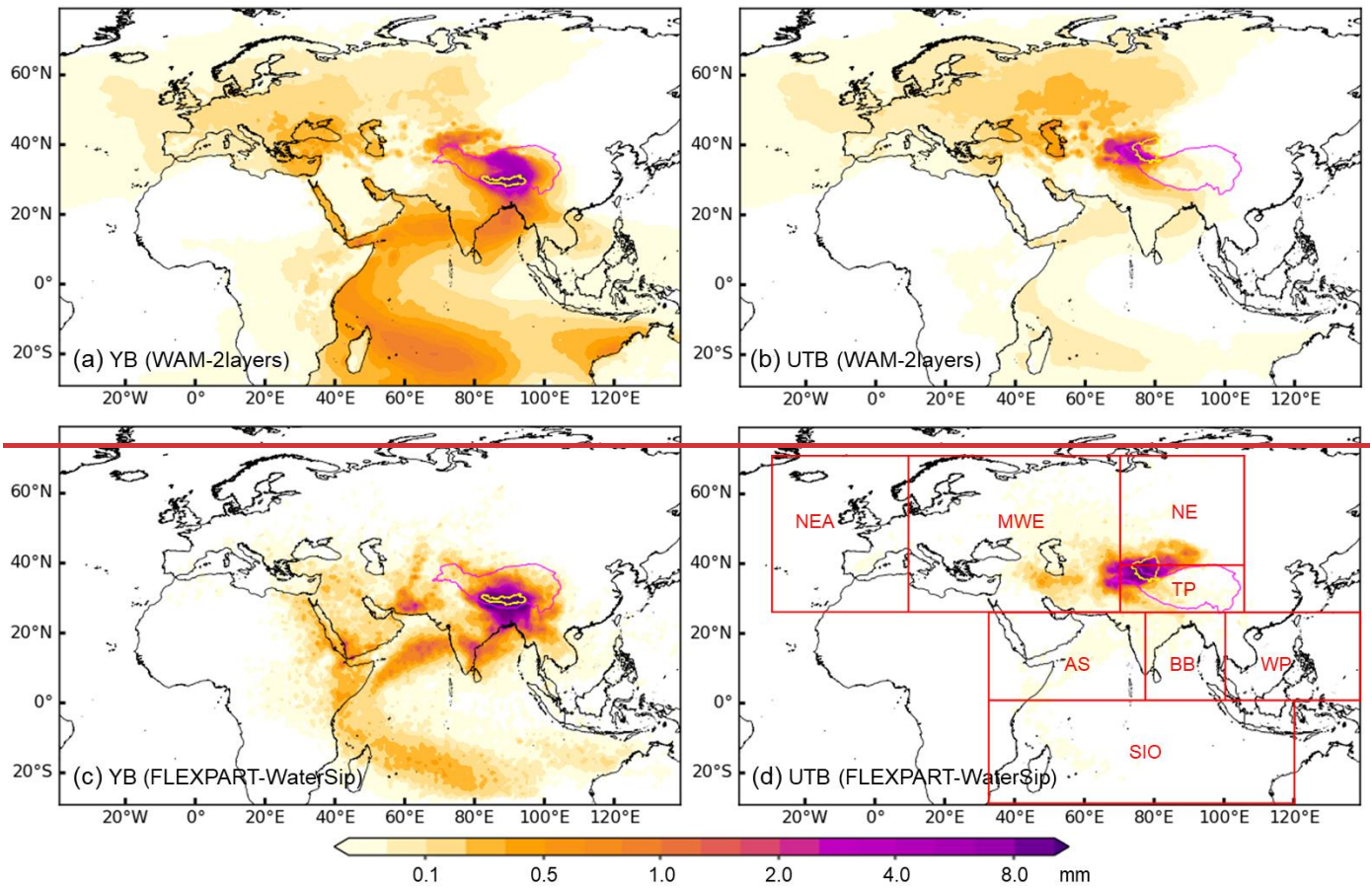
Figure 3: Spatial distributions of moisture contributions (equivalent water height over source regions; mm) to precipitation in July 2022 in the (a and c) YB and (b and d) UTB simulated by (a and b) WAM-2layers and (c and d) FLEXPART-WaterSip models. Purple lines represent the TP boundary and yellow lines represent the boundaries of the two representative basins. Red boxes in (d) delineate the eight source regions: Northeastern Atlantic (NEA), Midwestern Eurasia (MWE), Northern Eurasia (NE), TP, Arabian Sea (AS), Bay of Bengal (BB), Western Pacific (WP), and Southern Indian Ocean (SIO).

The differences between the moisture tracking results from the two models are shown in Figure 4 (WAM-2layers minus FLEXPART-WaterSip). Compared to FLEXPART-WaterSip, WAM-2layers model tends to estimate a higher moisture contribution from the westerlies-dominated northwestern source regions for both basins, spanning from nearby sources northwest of the YB and west of the UTB to distant sources across the entire northwestern Eurasian continent and northeastern Atlantic. Additionally, WAM-2layers model estimates greater moisture contributions from large parts of the Indian Ocean, particularly the distant Southern Indian Ocean in the YB simulation. In contrast, lower contributions estimated by WAM-2layers are mainly from local and nearby source regions downwind of the westerlies, specifically around the southern slopes of the Himalayas in the YB simulation and the entire Tarim Basin in the UTB simulation. Notably, over the Red Sea and

Persian Gulf regions, WAM-2layers model indicates higher moisture contributions from the oceans but lower moisture

205    contribution from the surrounding lands than FLEXPART-WaterSip, especially in the YB simulation (Fig. 4a). These discrepancies between the two moisture tracking models are consistent both in absolute and relative terms (Figs. 4 and S2).
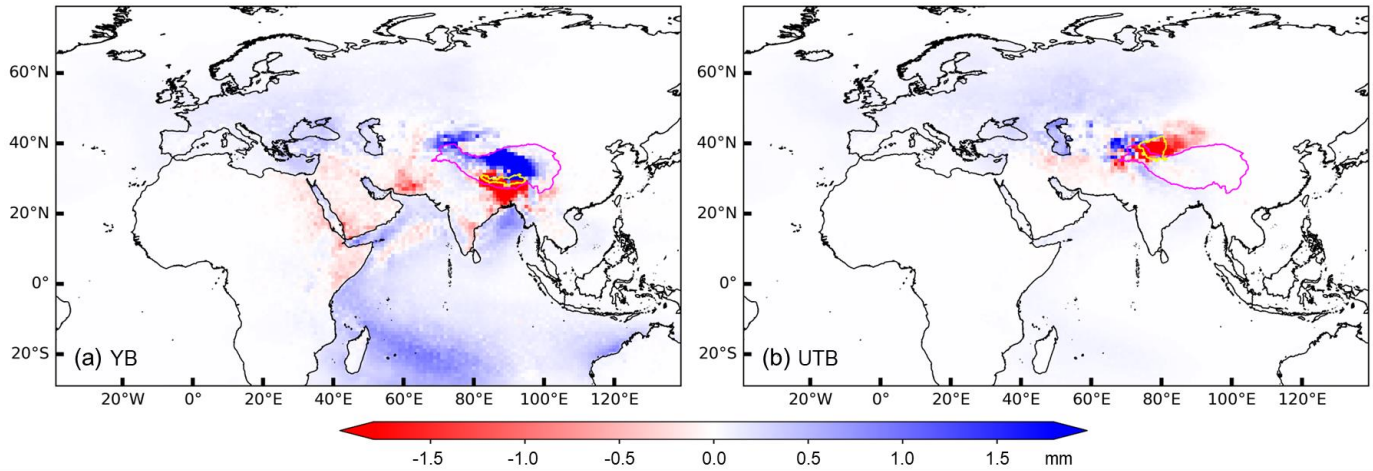
**Figure 4: Absolute differences in moisture contributions to precipitation in July 2022 between WAM-2layers and FLEXPART-WaterSip (WAM-2layers minus FLEXPART-WaterSip) for the (a) YB and (b) UTB simulations.**

210

Considering the distribution of moisture sources, eight critical source regions (see the red boxes in Fig. 3d) are selected for further quantitative analysis. Figure 5 shows the relative contributions from the eight critical regions and remaining regions to precipitation in the YB and UTB. Both models indicate that the major moisture sources for the YB are local recycling and the ISM regions (TP, AS, BB, and SIO), whereas for the UTB, the primary sources are local recycling and westerlies-influenced

215    regions (TP, NE, and MWE). Specifically, WAM-2layers model estimates that the TP contributes 32% of the moisture toward the YB, which is about two-thirds of the estimate by FLEXPART-WaterSip model (53%). An even greater discrepancy is observed for the contribution of the TP to the UTB, for which WAM-2layers model estimates 28% compared to FLEXPART-WaterSip's 72%. For distant sources, the SIO is the most representative one for the YB, with WAM-2layers estimating its contribution at 30%, compared to only 11% by FLEXPART-WaterSip. For the UTB, the MWE is a key distant source, with

220    WAM-2layers estimating a 36% contribution, doubling that calculated by FLEXPART-WaterSip (15%). In summary, compared to FLEXPART-WaterSip, WAM-2layers model generally estimates higher moisture contributions from the westerlies-dominated sources as well as distant sources, but lower contributions from local recycling and nearby sources downwind of the westerlies.
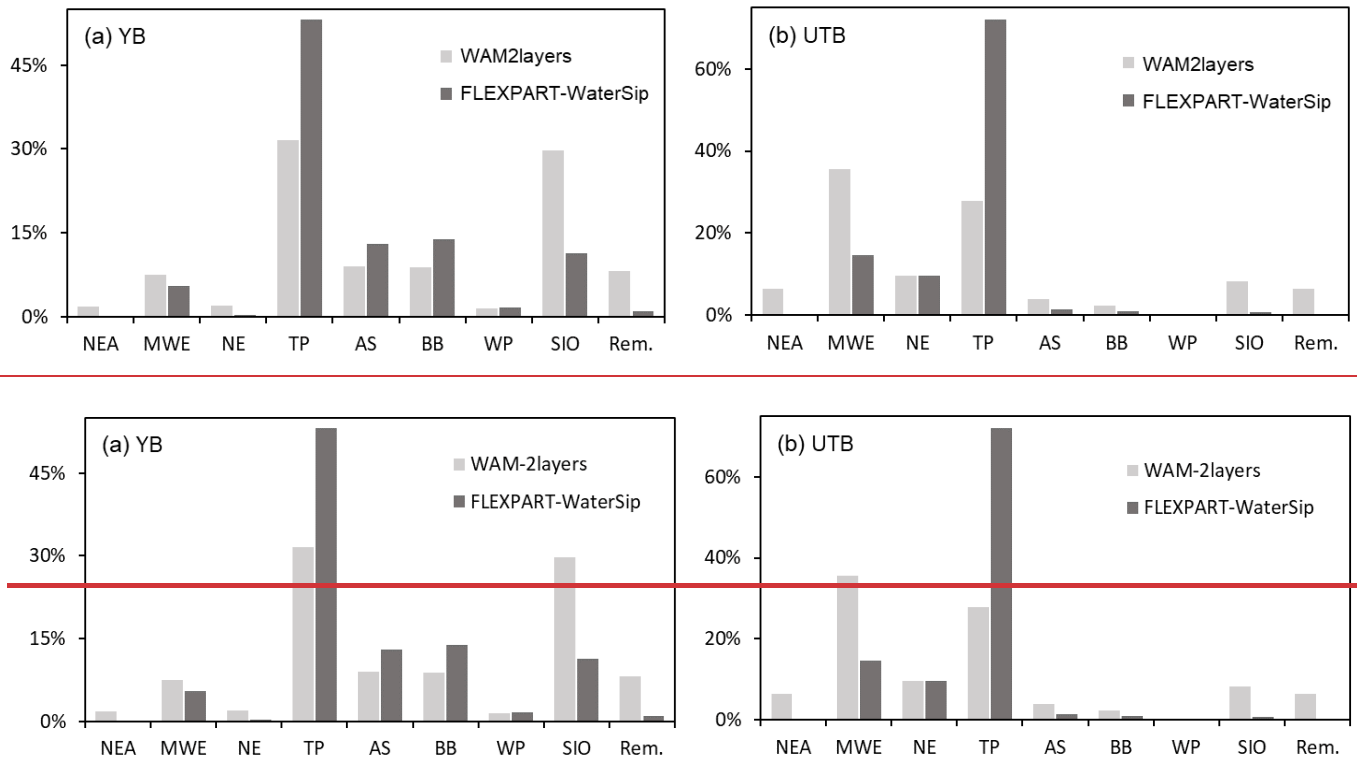
225

**Figure 5: Relative moisture contributions (%) to precipitation in July 2022 over the (a) YB and (b) UTB from the eight selected source regions (NEA, MWE, NE, TP, AS, BB, WP, and SIO) and the remaining (Rem.) source regions simulated by WAM-2layers and FLEXPART-WaterSip models.**

## 4 Moisture fluxes in WAM-2layers and particle trajectories in FLXPART-WaterSip simulations

230 When tracing moisture sources, WAM-2layers model primarily utilizes horizontal moisture fluxes in the upper and lower atmospheric layers to determine the water vapor transport from global sources to the target region in a backward mode. Figure 6 illustrates the average moisture transport fluxes in the two layers during the entire simulation period as estimated by WAM-2layers. The ISM-dominated moisture transport to the TP region primarily occurs in the lower layer, whereas the westerlies-dominated moisture transport to the region is mainly from the north in the lower layer and from the west in the upper layer, a

235 phenomenon pronounced in the northwest vicinity of the UTB.
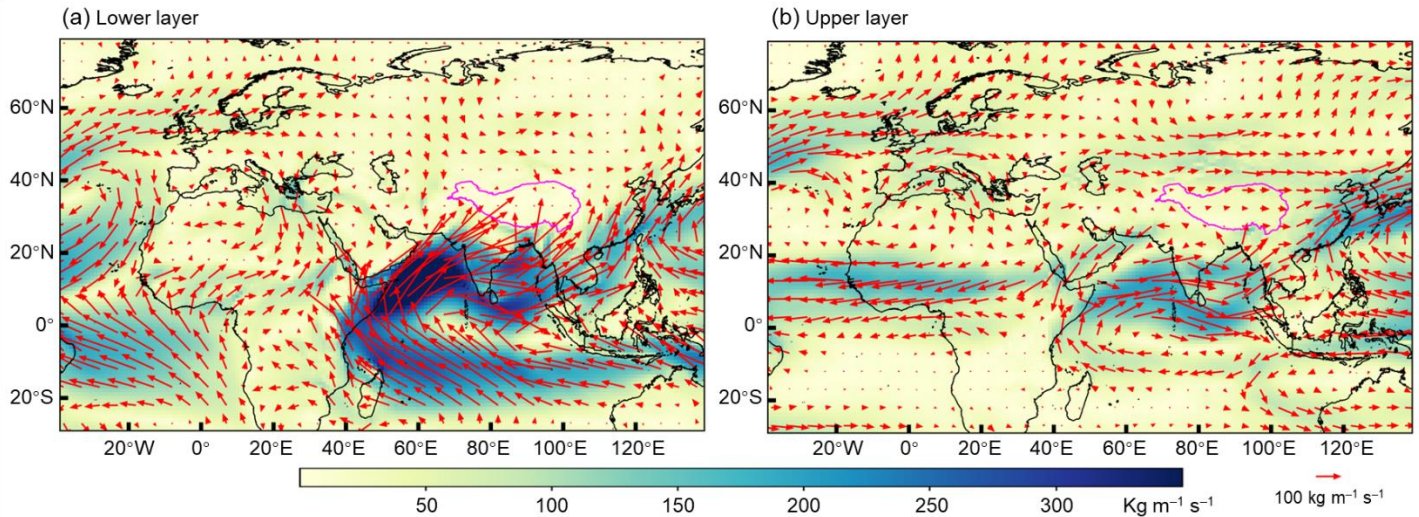
**Figure 6: Average moisture transport fluxes (kg m⁻¹ s⁻¹) in the (a) lower and (b) upper layers in WAM–2layers during the entire simulation period (June–July 2022).**

In comparison, FLEXPART outputs detailed information on air particles and trajectories critical to diagnosing moisture sources. Figure 7 shows the spatial distributions of particles and trajectories contributing to precipitation over the YB and UTB in the FLEXPART-WaterSip simulation. It should be noted that the particles and trajectories in Fig. 7 are clustered results using the K-means clustering method for clearer graphical representation, reducing the number of particles by a factor of 100 and the number of trajectories by a factor of 150. This treatment may have filtered out some chaotic and distant particles and trajectories. In Lagrangian backward simulations, particles released from the YB predominantly travel southwestward, while those from the UTB primarily spread westward (Fig. 7a and b). Within about 15 days, the traced particles can reach the farthest source regions. The results of backward tracking days suggest approximately three distinct, fastest moisture transport paths to the YB: the northwestern route from the MWE, the southwestern route from the AS, and the southeastern route from the WP. The most pronounced moisture transport path to the UTB is confined to western routes. Additionally, there is a notable rapid northeastward transport of tracked particles in the UTB over a short period after release (Fig. 7b and Fig. 3d), a phenomenon indiscernible in WAM–2layers simulations (Fig. 3b and d and Fig. 6). This phenomenon may be associated with the complex and variable convective activities as well as the simulation biases in the region, as indicated by the vertical wind patterns at different pressure levels across the study domain (Fig. S3 in the Supplement) and the overestimated local evaporation in FLEXPART-WaterSip (see Sections 5 and 6).
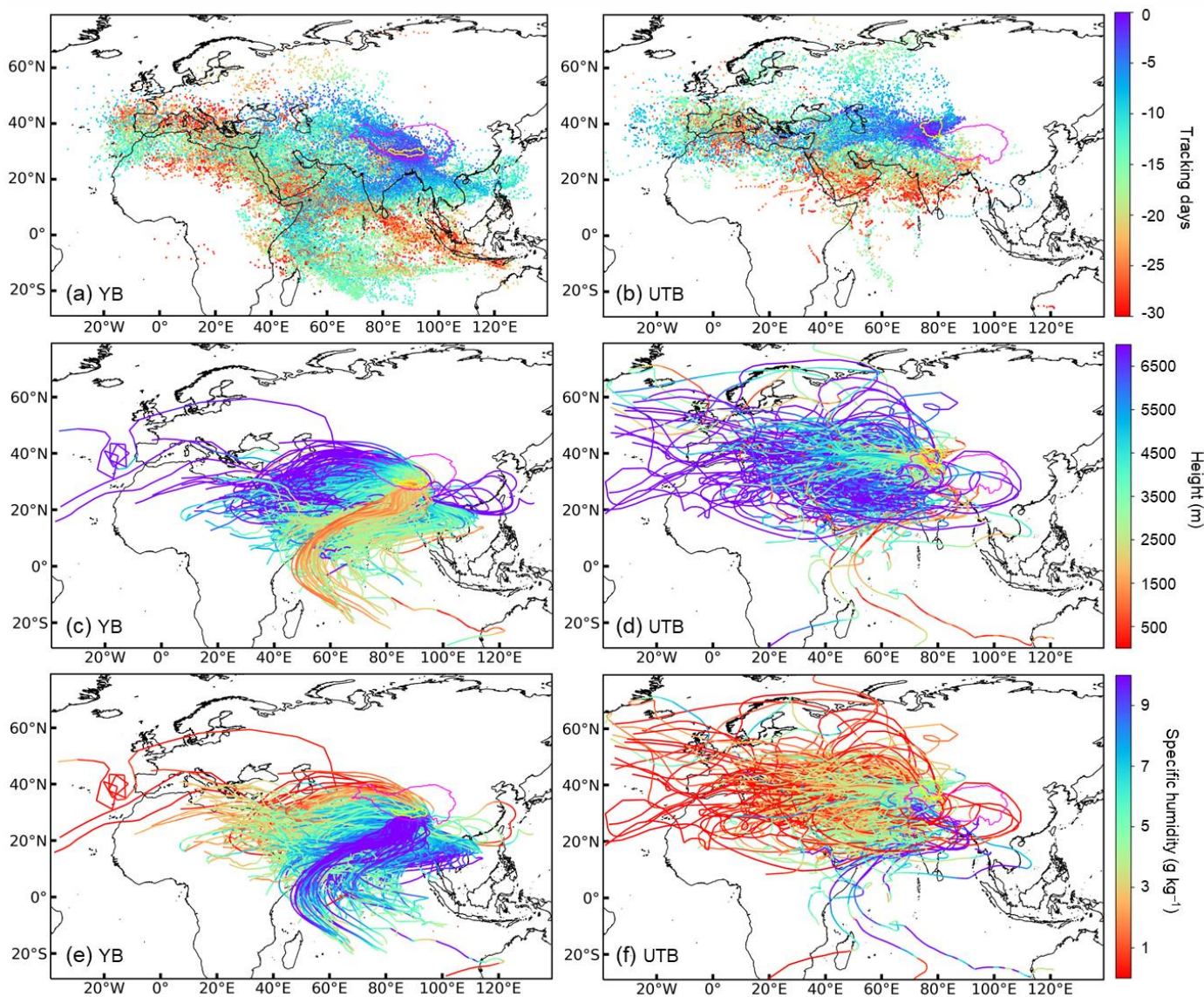
255

**Figure 7: Spatial distributions of (a and b) particles and (c–h) trajectories that transport moisture to the (a, c, and e) YB and (b, d, and f) UTB as simulated in FLEXPART model: (a and b) particles color-coded by backward-tracking days (0–30 days), (c and d) trajectories color-coded by height (m, above ground) at each numerical step, and (e and f) trajectories color-coded by specific humidity (g kg⁻¹) at each numerical step.**

260

As suggested in Fig. 7c–d, trajectories originating from the western sources are typically at higher altitudes, some even exceeding 6000 m, but they notably descend before reaching the target region, forming a strip-like lower atmospheric transport channel in the western part of the target region. This is in general consistent with WAM-2layers simulations, in which the upper-layer horizontal transport of moisture originating from the northwestern Eurasian is higher than that in the lower layer

(Fig. 6). In comparison, trajectories from the ISM-dominated sources are at relatively lower altitudes, with some originating from the SIO even descending below 1000 m. Generally, the moisture-carrying capacity of these trajectories correlates with both their altitude and the moisture conditions in their source regions. As shown in Fig. 6e–f, trajectories from the ISM-dominated regions and lower altitudes exhibit higher moisture content, whereas those from the westerlies-dominated regions and higher altitudes are characterized by lower moisture content.

A notable difference between WAM–2layers and FLEXPART-WaterSip simulations, as illustrated in Fig. 4, is that the spatial extent of source regions identified in FLEXPART-WaterSip is much smaller than in WAM–2layers, especially in distant regions such as northwestern Eurasia. Particle trajectories simulated by FLEXPART are only sparsely distributed across northwestern Eurasia, particularly for the YB (Fig. 7). This inconsistency is also evident when comparing previous studies using WAM–2layers (Zhang et al., 2017; Li et al., 2022a) and FLEXPART-WaterSip (Chen et al., 2019; Yao et al., 2020). This indicates that the underestimated moisture contributions from these distant sources in FLEXPART-WaterSip, as compared to WAM–2layers, are largely due to a lower proportion of particles originating from these source regions reaching the target region.

## 5 Relationship between "actual evaporation" and simulated moisture contributions

In general, for moisture source–receptor diagnostics within a specific source region, areas with higher evaporation rates generally contribute more moisture to the target region than areas with lower rates, especially where the contrast between oceanic and terrestrial evaporation is pronounced. To further investigate the relationship between evaporation and simulated moisture contributions from various source regions, we employ evaporation data from ERA5 as the benchmark ("actual evaporation"; Fig. 8a) for the entire tracking period (June–July 2022). As shown in Figs. 3 and 8a, the distribution of moisture sources simulated by WAM–2layers aligns more closely with global evaporation patterns from ERA5 (oceanic evaporation rates exceed those of surrounding terrestrial areas) compared to that by FLEXPART-WaterSip. This alignment is particularly evident in the Red Sea and Persian Gulf regions, where one of the most pronounced discrepancies between the two models is observed (Fig. 4a).
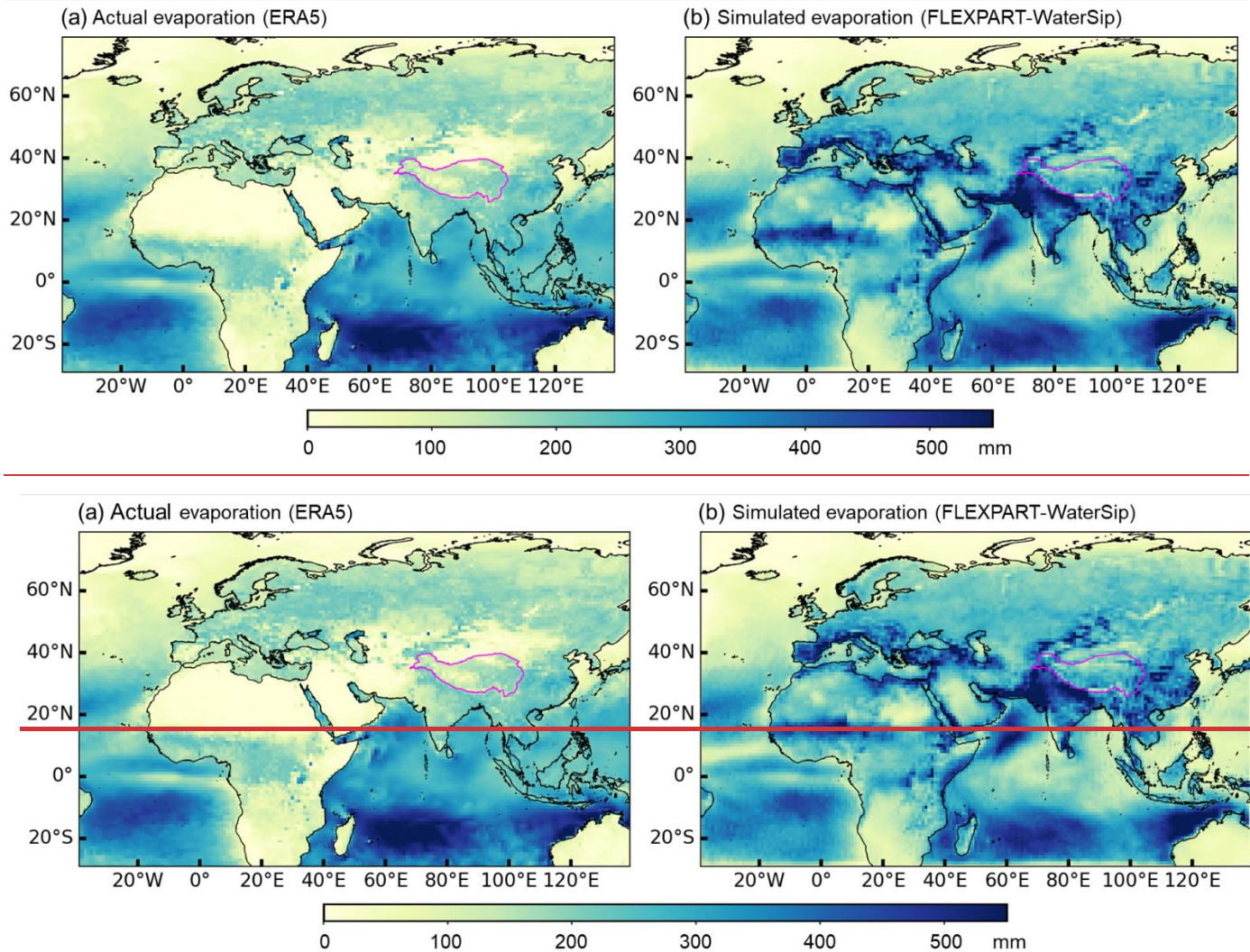
**Figure 8: (a) Evaporation from ERA5 and (b) simulated evaporation from FLEXPART-WaterSip during June–July 2022.**

We then examine the relationship between "actual evaporation" and simulated moisture contributions across all grid cells in the eight selected source regions (Fig. S4). It is clear that, for both basins, positive correlations between "actual evaporation" and moisture contributions mainly appears in WAM-2layers simulations, especially in the westerlies-dominated NEA and MWE as well as the ISM-dominated AS and SIO regions, where correlation coefficients all exceed 0.3. In contrast, FLEXPART-WaterSip simulations rarely show strong positive correlations between "actual evaporation" and moisture contributions. A striking example is the Red Sea and Persian Gulf regions where oceanic evaporation is notably higher than terrestrial evaporation (Fig. 8a). As mentioned above, FLEXPART-WaterSip model appears to inadequately capture the relatively high evaporation over the Red Sea, Persian Gulf, and eastern Mediterranean (see Fig. 3c), despite extensive tracking

particles in these regions (see Fig. 7a). We speculate that the complex atmospheric activities in these regions, as partially evidenced by vertical velocities in Fig. S3, may contribute to these issues in moisture source diagnosis using the WaterSip method. Some earlier studies have also indicated that this method is prone to misidentifying the convergence/divergence processes (Winschall et al., 2014; Cloux et al., 2021), particularly a study over the Sahara has further emphasized the importance of cloud microphysical processes as well as dry and moist convection embedded in the heat low (Dahinden et al., 2023). To further illustrate the underlying mechanisms, we randomly selected two representative trajectories: one from the SIO to the YB, and the other from the NEA to the UTB (Fig. S5 in the Supplement). Comparisons between model outputs and ERA5 data, as shown in Fig. S6 in the Supplement, suggest that the modeled changes in specific humidity for particles may not fully reflect the actual processes of precipitation and evaporation during the moisture transport. Relying solely on specific humidity changes and particle height to assess evaporation, precipitation, and moisture transport can be quite challenging. Although the WaterSip method employs thresholds (e.g., 1.5 BLH and 0.2 $g^{-1}\,kg^{-1}$ every 6 h for specific humidity changes) to exclude a large number of potential misdiagnoses over the source regions, further advancements in diagnostic and correction methods are still needed.

Similar to the moisture source-receptor diagnosis for precipitation particles in the target area, computing all released particles in the atmosphere would provide simulated evaporation over the entire tracking domain. Therefore, Fig. 8b displays the FLEXPART-WaterSip simulated evaporation over the tracking domain during the entire tracking period. In comparison with "actual evaporation", FLEXPART-WaterSip model generally captures the spatial pattern of evaporation across oceanic regions but largely overestimates terrestrial evaporation from mid- and low-latitudes (e.g., surrounding the Mediterranean, the Middle East, and the Indian subcontinent; all of which are critical source regions for the two basins in the TP). These findings are consistent with a previous long-term, global scale study by Keune et al. (2022). Although FLEXPART-WaterSip demonstrates potential in capturing complex local atmospheric activities, the bias in simulated evaporation can inevitably affect the quantification of moisture source–receptor dynamics.

## 6 Bias correction of FLEXPART-WaterSip simulations

Keune et al. (2022) introduced the Heat And MoiSture Tracking framEwoRk (HAMSTER), a unified framework designed to correct biases in moisture source–receptor diagnostics based on particle trajectories from Lagrangian models. This framework leverages the relationships between actual and simulated surface fluxes (evaporation and precipitation). The first step, in line with WaterSip, is to use specific thresholds for specific humidity changes, relative humidity, and particle height to quantify moisture source–receptor relationships for precipitation in the target region (a "random attribution" method was also introduced). Subsequently, a first round of corrections is conducted by comparing actual and simulated precipitation in the target region (i.e., bias correction of receptor variables). A second round of corrections then focuses on comparing actual and simulated evaporation across all source regions (i.e., bias correction of source variables). These processes aim to achieve

reasonable, bias-corrected moisture source contributions. It is noteworthy that the HAMSTER method does not include calibration for the filtering thresholds of precipitation particles in the target region, potentially leading to certain deviations in

335 the spatiotemporal distribution of tracked particle trajectories. If actual precipitation data in the target region were used to calibrate the filtering thresholds of precipitation particles, the step of "bias correction of receptor variables" in HAMSTER could be replaced. Inspired by the HAMSTER method, we develop a simplified two-step approach to correct moisture tracking results from FLEXPART-WaterSip:

340 **Step 1:** Optimize the filtering thresholds of precipitation particles in the target region. Using the default precipitation particle filtering thresholds for specific humidity change ($0.2 \text{ g kg}^{-1}$) and relative humidity (80%), we conducted numerical experiments to examine how adjustments to these thresholds impact simulated precipitation. As shown in Fig. 9a and b, maintaining a constant relative humidity threshold at 80% while varying the specific humidity change threshold from 0.05 to $0.2 \text{ g kg}^{-1}$ results in a minimal decrease in simulated precipitation (less than 1 mm for both basins). In contrast, fixing the specific

345 humidity change threshold at $0.2 \text{ g kg}^{-1}$ while changing the relative humidity threshold leads to substantial changes in simulated precipitation (Fig. 9c and d). Our experiments indicate that precipitation simulation is more sensitive to changes in the relative humidity threshold, with the optimal values of 63% for the YB and 74% for the UTB. This step ensures a more accurate selection of precipitation particles for subsequent moisture source diagnosis.
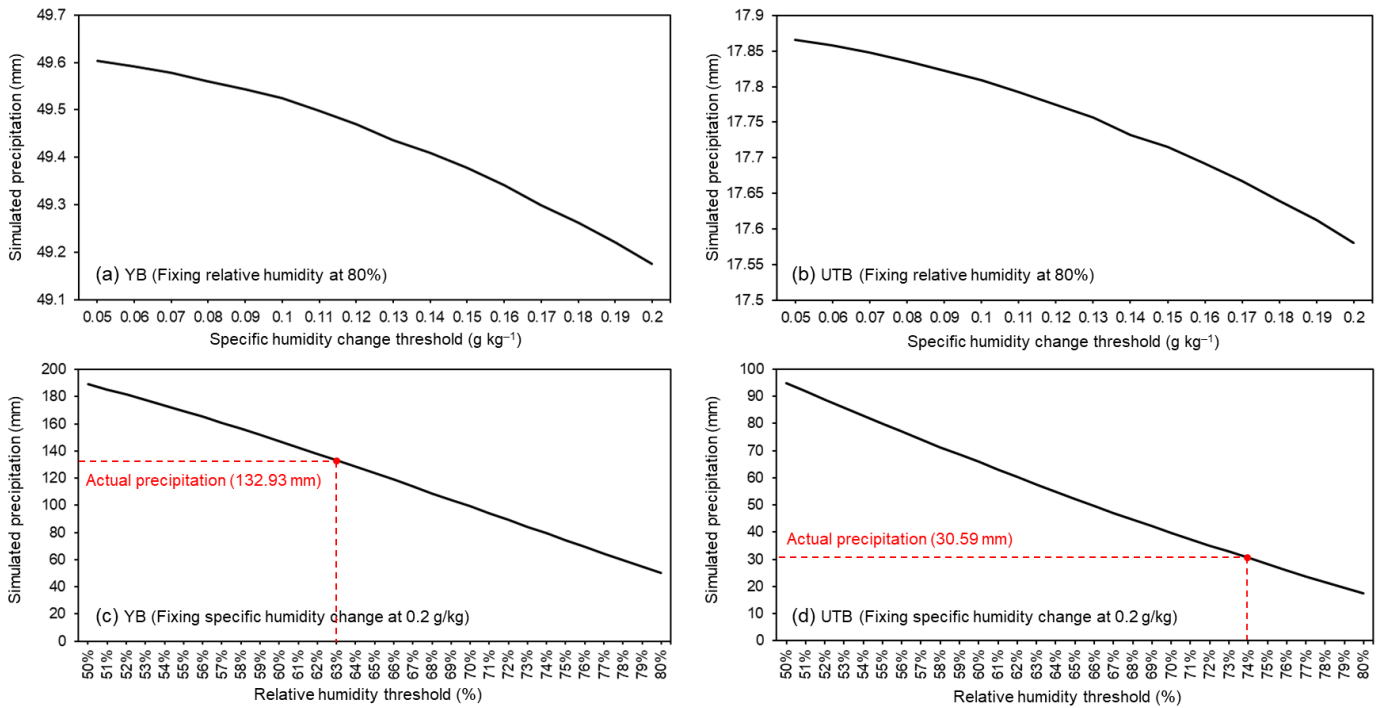
350 **Figure 9: Sensitivity of the simulated precipitation in the (a and c) YB and (b and d) UTB to (a and b) the threshold of specific humidity change and (c and d) the threshold of relative humidity.**

**Step 2:** Correct biases in simulated evaporation over the source regions. First, use the optimized thresholds from Step 1 to quantify moisture source contributions. Next, calculate grid-scale correction factors by dividing actual evaporation by

355    simulated evaporation for each grid cell over the entire moisture tracking period (Fig. S7 in the Supplement). These correction factors are then applied to correct moisture source contributions. This step addresses the simulation biases in evaporation across the moisture tracking domain when using the WaterSip method. It is important to note that although these correction factors are likely to vary over time, this variability was not accounted for in this study due to the relatively short simulation period. For long-term moisture source diagnosis corrections, implementing time-varying correction factors would be more

360    appropriate.

The bias-corrected FLEXPART-WaterSip simulations for the YB and UTB, based on the two-step bias correction approach, are shown in Fig. 10a and b. The bias correction align the FLEXPART-WaterSip simulation results more closely with the global pattern of terrestrial and oceanic evaporation, especially around the Red Sea and Persian Gulf regions. Additionally, it

365    enhances the moisture contributions from the high-latitude Eurasian continent and the Indian Ocean, while reducing contributions from the western land areas in the mid- and low-latitude (Fig. S7 in the Supplement). We further compare these bias-corrected simulations with the original WAM-2layers and FLEXPART-WaterSip simulations, as shown in Fig. 10c–f. The differences depicted in Fig. 10c–d are generally consistent with those in Fig. 4, indicating that WAM-2layers model tends to estimate higher moisture contributions from the westerlies-dominated sources and distant sources, but lower contributions

370    from local recycling and nearby sources downwind of the westerlies for both the YB and UTB. Compared to the bias-corrected results, the original (uncorrected) FLEXPART-WaterSip simulations for the YB estimate lower moisture contributions from areas surrounding the target region and oceanic source regions, but higher contributions from the western land areas (Fig. 10e). For the UTB, the uncorrected FLEXPART-WaterSip simulations mainly estimate higher moisture contributions from the target region and its surrounding areas (Fig. 10f), including the northeastward stretch of moisture sources observed in Fig. 3d. These

375    comparisons demonstrate that through bias correction, the original discrepancies in reflecting actual evaporation between WAM-2layers and FLEXPART-WaterSip simulations can be significantly mitigated.
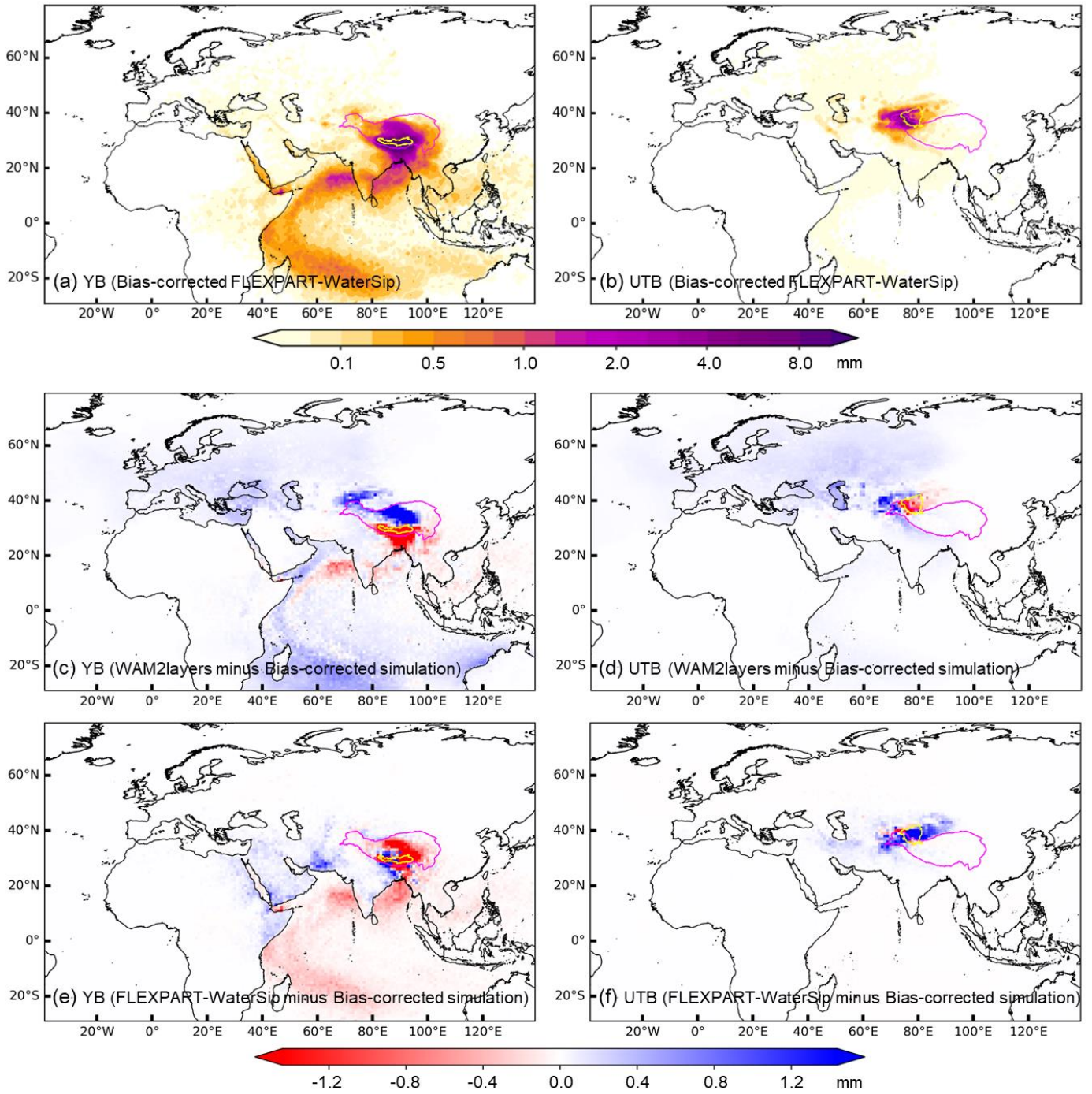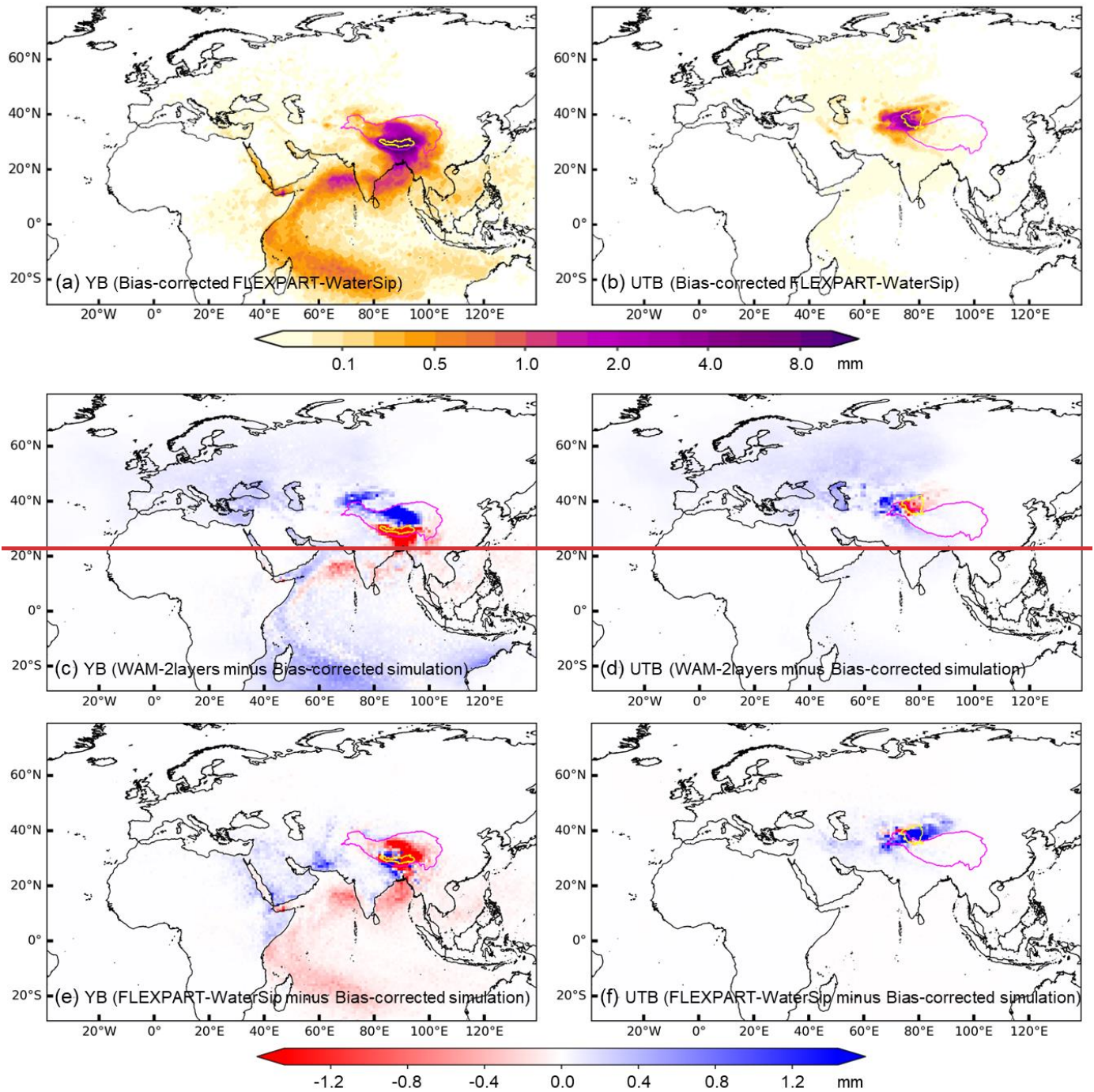
**Figure 10: (a and b)** Spatial distributions of bias-corrected moisture contributions (equivalent water height over source regions; mm)
to precipitation in July 2022 in the **(a)** YB and **(b)** UTB simulated by FLEXPART-WaterSip model. **(c–f)** Absolute differences in

moisture contributions between original WAM-2layers/FLEXPART-WaterSip simulations and bias-corrected FLEXPART-WaterSip simulations for the (c and e) YB and (d and f) UTB.

## 7 Potential determinants of discrepancies in moisture tracking

We now turn to a more comprehensive examination of the discrepancies observed in the original WAM-2layers and
385 FLEXPART-WaterSip simulations. Considering the underlying physics of the models, forcing datasets, parameter selections, and our computational resources, we designed four sets of numerical experiments to investigate potential factors contributing to the discrepancies in different simulations.

**Experiment 1 – model resolution:** Simulation of moisture sources using WAM-2layers is essentially a dynamic reproduction
390 of moisture transport conditions based upon forcing datasets, which means that the accuracy heavily depends on the spatial and temporal resolutions of input data. In addition to the original settings (1°×1° at 3-hourly resolution), we introduce three additional configurations of ERA5 data to determine whether improved spatial and/or temporal resolutions in forcing data could provide more accurate moisture source attributions: 1°×1° at hourly resolution, 0.25°×0.25° at 3-hourly resolution, and 0.25°×0.25° at hourly resolution. The results from these additional simulations are summarized in Fig. S8 in the Supplement.
395

**Experiment 2 – moisture source diagnosis thresholds:** Quantifying moisture source–receptor relationships in FLEXPART-WaterSip hinges on the diagnosis of potential precipitation particles and evaporation sources, which in turn depends on a set of threshold settings. Previous studies have suggested that optimal configurations for these thresholds may vary globally (Sodemann et al., 2008; Fremme and Sodemann, 2019; Keune et al., 2022). In addition to the original setting (a relative
400 humidity threshold of 80% and a specific humidity change threshold of 0.2 g kg$^{-1}$), we introduce one additional configuration for precipitation particles selection using the optimized relative humidity threshold for the YB and UTB (63% and 74%, respectively), and two additional configurations for evaporation source identification with specific humidity change threshold set at 0.1 and 0 g kg$^{-1}$. The results from these additional simulations are summarized in Fig. S9 in the Supplement.

405 **Experiment 3 – number of particles:** Using particle trajectories for source diagnostics inevitably limits the identified moisture sources to these trajectories. Consequently, a lower number of trajectories may result in potential inaccuracies, particularly when representing small to medium-scale atmospheric processes. This numerical experiment is designed to determine whether the relatively sparse particle trajectories over distant source regions could introduce substantial uncertainties when estimating moisture contributions in FLEXPART-WaterSip. In this experiment, we reduce the number of particles
410 initially released in FLEXPART from five million to one million. The results of this experiment are summarized in Fig. S10 in the Supplement.

**Experiment 4 – "areal source–receptor attribution" method:** Different from the WaterSip method proposed by Sodemann et al. (2008), which attributes precipitation at a specific point within the target region to moisture uptake from multiple points along the trajectories, Sun and Wang (2014) introduced the "areal source–receptor attribution" method, focusing on a regional rather than a point scale. The "areal source–receptor attribution" method calculates the total moisture contribution from an examined source to precipitation across the entire target region instead of at specific points. It facilitates the differentiation of moisture contributions from within and outside the examined sources along the trajectories. The basic framework of the "areal source–receptor attribution" method is shown in Fig. S11 in the Supplement, and the detailed methodology can be found in Sun and Wang (2014). In this numerical experiment, we apply "areal source–receptor attribution" method to quantify moisture contributions from the eight source regions.
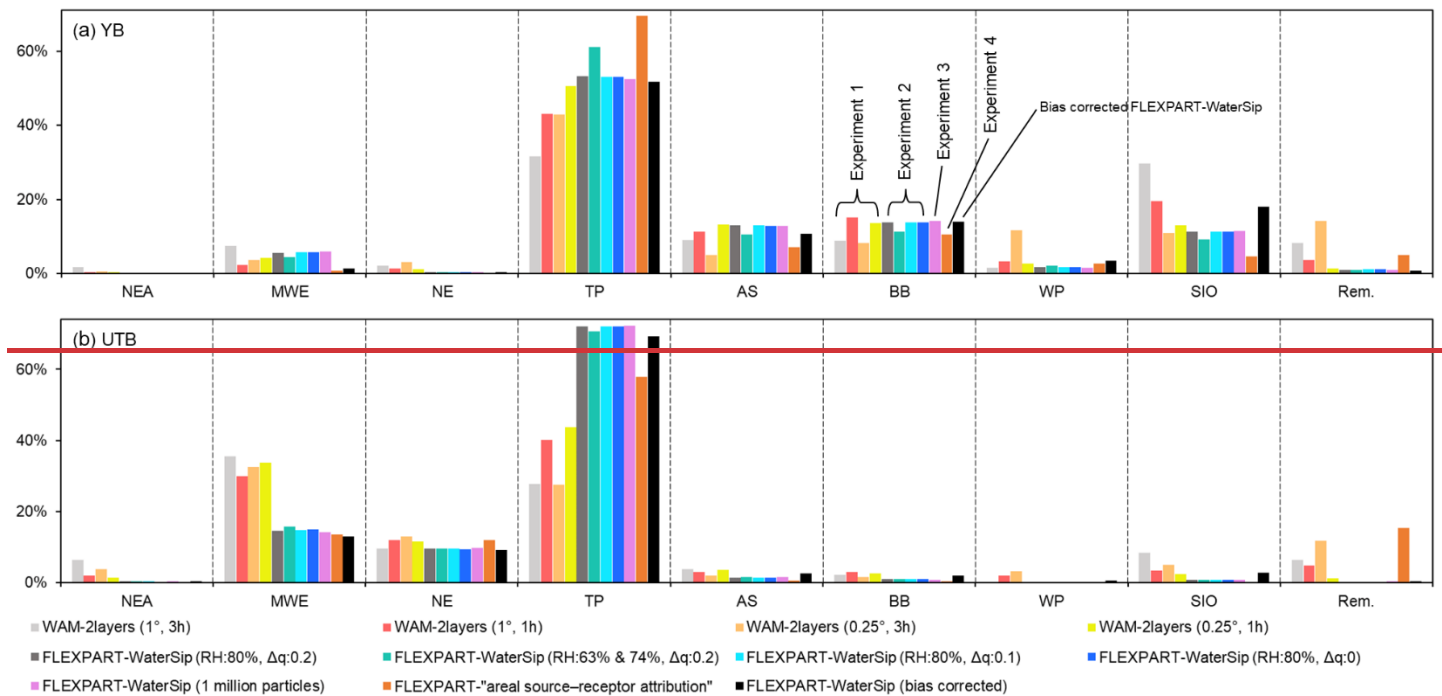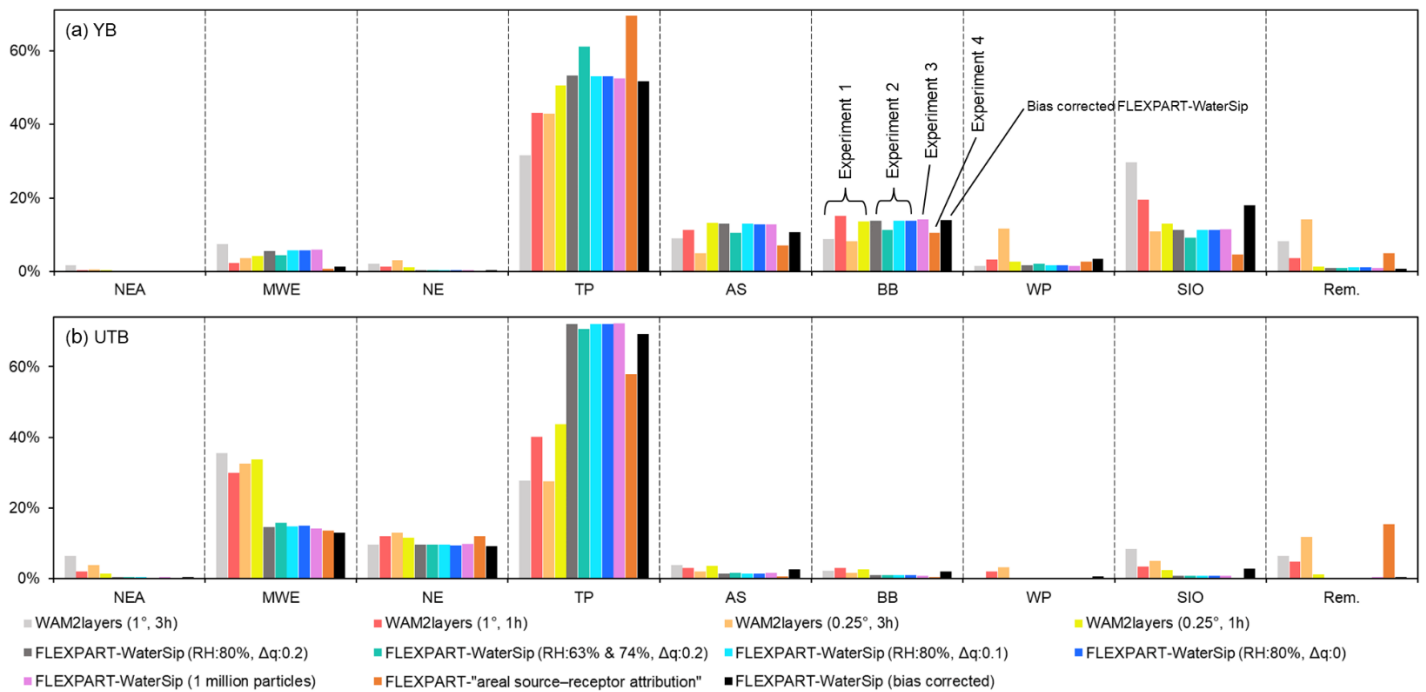
**Figure 11: Relative moisture contributions (%) to precipitation over the (a) YB and (b) UTB from the eight selected source regions**
425 **and the remaining (Rem.) source regions simulated by four sets of numerical experiments (including different configurations in**

**WAM‑2layers and FLEXPART-WaterSip and FLEXPART-"areal source–receptor attribution") as well as the bias-corrected FLEXPART-WaterSip simulations. Black histograms represent the bias-corrected FLEXPART-WaterSip simulations. RH and Δq represent relative humidity threshold and specific humidity change threshold (g kg⁻¹), respectively. Experiments 1–4 correspond to numerical experiments focusing on model resolution, moisture source diagnosis thresholds, number of particles, and "areal source–receptor attribution" method.**

Figure 11 shows the relative moisture contributions from the eight selected source regions and the remaining source regions to the YB and UTB in the four set of numerical experiments and the bias-corrected FLEXPART-WaterSip simulations. The results for each source region includes 11 sets of simulations, including original simulations in Section 3 and the bias-corrected simulations in Section 6. In Experiment 1, increasing the spatial and temporal resolutions of the forcing dataset in general aligns WAM‑2layers simulations more closely with the bias-corrected FLEXPART-WaterSip (e.g., see results with 0.25°×0.25° at hourly resolution in Fig. S8e and f in the Supplement), particularly for the YB. For nearby sources, moisture contributions from the TP to the YB (UTB) increases from 32% (28%) to 51% (44%). For distant sources, contributions from the SIO and MWE to the YB (UTB) decrease from 30% (8%) to 13% (2%) and from 7% (36%) to 5% (34%), respectively. Our sensitivity experiments for temporal and spatial resolutions reveal that increasing temporal resolution (from 3h to 1h) substantially enhances the reliability of moisture source simulations (Fig. S8a–b in the Supplement). This aligns with prior knowledge that models with finer temporal resolution are better at capturing atmospheric perturbations, which could be of significant importance for moisture tagging (van der Ent et al., 2013). In contrast, solely increasing spatial resolution (from 1° to 0.25°) may lead to a stronger eastward extension of moisture sources for both basins (Fig. S8c–d in the Supplement), which is inconsistent with WAM‑2layers (0.25°, 1h) and bias-corrected FLEXPART-WaterSip results. In addition to spatiotemporal resolutions, van der Ent et al. (2013) previously summarized that the two primary factors affecting the WAM2layers simulations are the moisture weighted well-mixed assumption and the method used to handle wind shear and turbulence. However, addressing these issues is beyond the scope of this work. Moreover, Tuinenburg and Staal (2020) advised caution regarding the large moisture fluxes relative to Eulerian grid cells as well as the use of smaller time steps to mitigate numerical dispersion. ~~Overall~~Overall, Experiment 1 demonstrates that improving the spatiotemporal resolutions of forcing data in WAM‑2layers can mitigate the underestimation of nearby sources and overestimation of distant sources for both basins, particularly for the YB. ~~(Tuinenburg and Staal, 2020)~~

In Experiment 2, adjusting the thresholds of relative humidity substantially enhances the overall moisture contributions from the source regions to both basins of the TP, yet it has minimal effect on the spatial patterns of moisture sources (Fig. S9a–b in the Supplement). Sensitivity experiments on specific humidity change threshold show only a slight impact on moisture source simulations for the two basins (Fig. S9c–f in the Supplement). Generally, modifying the thresholds of moisture source–receptor diagnostics does not seem to reduce the potential biases in the spatial distributions of moisture sources when compared to the bias-corrected FLEXPART-WaterSip. In Experiment 3, reducing the number of released particles somewhat limits our ability

460 to discern finer details in the spatial distribution of moisture sources (Fig. S10 in the Supplement), although the quantified moisture contributions closely resemble those in the original FLEXPART-WaterSip simulations with 5 million particles. This is in line with a previous study showing that the Lagrangain model is not very sensitive to the number of particles once a certain threshold is reached (Tuinenburg and Staal, 2020). In Experiment 4, unlike the WaterSip method, the "areal source–receptor attribution" method utilizes all simulated trajectories for moisture source diagnosis, which may accumulate errors in

465 trajectories that do not result in precipitation in the target region. Reapplying the "areal source–receptor attribution" method with trajectories filtered by the WaterSip method can produce moisture contributions that more closely align with the FLEXPART-WaterSip estimates (results not shown). Overall, these sensitivity experiments underscore that current approaches to diagnosing moisture sources for the TP using numerical moisture tracking models still hold substantial potential for improvement and refinement.

470 **8 Discussion and conclusions**

Over the past few decades, considerable efforts have been made to identify and quantify the contributions of moisture sources to precipitation over the TP. A synthesis of these studies indicates that the most commonly used Eulerian and Lagrangian moisture tracking models are WAM-2layers and FLEXPART-WaterSip, respectively. However, the suitability and reliability of these models for moisture tracking over the TP, especially the potential discrepancies in moisture tracking results, have not

475 yet been thoroughly examined. This study addresses this gap by focusing on two representative basins of the TP: the YB (representing the ISM-dominated regions) and the UTB (representing the westerlies-dominated regions). Moisture source contributions to precipitation over these two basins were tracked using both WAM-2layers and FLEXPART-WaterSip models. We then investigated the discrepancies in moisture tracking results between these two models and their potential determinants through comparisons with actual evaporation, bias correction, and a set of sensitivity experiments.

480

The WAM-2layers model, designed for moisture tracking based on the water balance equation at a spatial-temporal resolution constrained by the forcing dataset, may face challenges in accurately capturing moisture transport to target regions through smaller-scale atmospheric processes. Compared with FLEXPART-WaterSip, the application of WAM-2layers over the TP is more computationally efficient. A notable pattern in WAM2layers, when compared~~persistent issue with WAM 2layers,~~

485 ~~relative~~ to the bias-corrected FLEXPART-WaterSip, is its tendency to estimate higher moisture contributions from westerlies-dominated sources and distant sources but lower contributions from local recycling and nearby sources downwind of the westerlies. However, this can be mitigated by utilizing higher spatial and temporal resolutions for forcing dataset in WAM-2layers, with a priority on improving temporal resolution, particularly in the ISM-dominated YB region. In addition, WAM-2layers offers one notable advantage over FLEXPART-WaterSip: its simulated spatial distribution of moisture sources is more

490 consistent with the pattern of actual evaporation, particularly around the Red Sea and Persian Gulf regions where the contrast between terrestrial and oceanic evaporation is strong.

The FLEXPART model, designed to track air particles in the atmosphere based on well-established physical mechanisms, is complemented by the WaterSip method to diagnose moisture source‐receptor relationships with information from simulated trajectories. FLEXPART-WaterSip enables us to investigate the movement of air particles transporting moisture in a detailed three-dimensional space. We investigated the potential impact of different filtering thresholds in the WaterSip method and varying numbers of released particles on moisture source–receptor diagnostics. The simulation of precipitation in the two basins is more sensitive to changes in relative humidity thresholds, while adjusting specific humidity change threshold does not significantly ~~alter~~ improve the estimated moisture source contributions. Nevertheless, the WaterSip method facilitates calibration of simulation biases by comparing results with ~~actual~~ observations (such as precipitation and evaporation). Therefore, if possible, we recommend bias-correcting the simulations from FLEXPART-WaterSip (through e.g., the method proposed by Keune et al. (2022) or the simplified two-step approach proposed in this study). The corrected results substantially reduce the evaporation biases over the source regions, particularly addressing the discrepancies arising from land–sea contrast in evaporation.

This study serves as a valuable reference for future numerical simulations aimed at tracking moisture sources across the TP region, including several crucial aspects such as model selection, error and uncertainty analysis, and strategies for improving simulation reliability~~enhancing simulate accuracy~~. While recognizing that each model is best suited to specific scenarios, this study highlights the critical need to account for the distinct characteristics of different models and the potential uncertainties in diagnosing moisture sources. Although this investigation is confined to short-term simulations using WAM‐2layers and FLEXPART-WaterSip models in two typical basins over the TP, it is anticipated that future research will extend such intercomparisons to other regions and even continental or global scale. Furthermore, in the field of numerical moisture tracking, it would be highly beneficial to explore the reliability of forcing data, incorporate additional physical moisture tracers (such as hydrogen and oxygen isotopes), and develop improved bias-correction methods for moisture source-receptor diagnosis.~~Furthermore, investigating the application of more sophisticated techniques for moisture source-receptor identification, particularly those that enhance the capability of Eulerian or Lagrangian models to capture small-scale atmospheric convection and turbulence, would be of significant benefit.~~

**Code availability.** The official website of WAM‐2layers is https://wam2layers.readthedocs.io/en/latest/ (version 3.0.0b5). The official website of FLEXPART is https://www.flexpart.eu/ (version 10.4). ~~The relevant code and installation tutorials can be obtained from these official websites. For the WaterSip method, the authoritative website is https://wiki.app.uib.no/gfi/index.php?title=WaterSip.~~ The WaterSip source code we developed in this study is available at https://doi.org/10.5281/zenodo.12780143. ~~can be found in Part 3 of the Supplement.~~ All additional algorithms are available on request from the first/corresponding author.

**Data availability.** ERA5 data are publicly available at the Climate Data Store (CDS) (https://cds.climate.copernicus.eu/). The input data of WAM-2layers were downloaded according to the example code in https://github.com/WAM2layers/WAM2layers/tree/main/scripts. The forcing data of FLEXPART were downloaded and pre-processed using the flex_extract v7.1.2 (https://www.flexpart.eu/flex_extract/). All simulation results in this study are available at https://doi.org/10.5281/zenodo.12780143.on request from the first/corresponding author.

**Author contributions.** YL conceptualized the study, carried out numerical simulations, conducted formal analysis, prepared figures, and wrote the initial draft. CW contributed to the editing, discussion, and interpretation. QT, SY, and BS provided comments on the manuscript. HP and SX provided supervision during the simulations and writing.

**Competing interests.** The contact author has declared that neither they nor their co-authors have any competing interests.

**Acknowledgements.** We thank Drs. Ruud van der Ent and Harald Sodemann for their invaluable and constructive feedback on earlier versions of this manuscript. We also thank the editor, Dr. Franziska Aemisegger, for her efficient handling and insightful feedback throughout the review process.We also thank the editor for their efficient handling and insightful feedback throughout the review process.

**Financial support.** This work was financially supported by the Second Tibetan Plateau Scientific Expedition and Research Program (grant no. 2019QZKK0207-02) and the Natural Science Foundation of Hubei Province of China (grant no. 2022CFB785). Q.T. was supported by the Third Xinjiang Scientific Expedition Program (grant no. 2021xjkk0805).

**References**

Ayantobo, O.O., Wei, J., Hou, M., Xu, J., Wang, G.: Characterizing potential sources and transport pathways of intense moisture during extreme precipitation events over the Tibetan Plateau, J. Hydrol. 615, 128734, https://doi.org/10.1016/j.jhydrol.2022.128734, 2022

Chen, B., Xu, X.D., Yang, S., Zhang, W.: On the origin and destination of atmospheric moisture and air mass over the Tibetan Plateau, Theor. Appl. Climatol. 110, 423-435, https://doi.org/10.1007/s00704-012-0641-y, 2012

Chen, B., Zhang, W., Yang, S., Xu, X.D.: Identifying and contrasting the sources of the water vapor reaching the subregions of the Tibetan Plateau during the wet season, Climate Dyn. 53, 6891-6907, https://doi.org/10.1007/s00382-019-04963-2, 2019

Chen, Y., Liu, B., Cai, X., Zhou, T., He, Q.: Moisture transport and sources of an extreme rainfall event of June 2021 in southern Xinjiang, China, Adv. Clim. Change Res. 13, 843-850, https://doi.org/10.1016/j.accre.2022.11.010, 2022

Cloux, S., Garaboa-Paz, D., Insua-Costa, D., Miguez-Macho, G., Pérez-Muñuzuri, V.: Extreme precipitation events in the Mediterranean area: contrasting two different models for moisture source identification, Hydrol. Earth Syst. Sci. 25, 6465-6477, https://doi.org/10.5194/hess-25-6465-2021, 2021

Curio, J., Scherer, D.: Seasonality and spatial variability of dynamic precipitation controls on the Tibetan Plateau, Earth Syst. Dynam. 7, 767-782, https://doi.org/10.5194/esd-7-767-2016, 2016

Dahinden, F., Aemisegger, F., Wernli, H., Pfahl, S.: Unravelling the transport of moisture into the Saharan Air Layer using passive tracers and isotopes, Atmospheric Science Letters 24, e1187, https://doi.org/10.1002/asl.1187, 2023

Fremme, A., Sodemann, H.: The role of land and ocean evaporation on the variability of precipitation in the Yangtze River valley, Hydrol. Earth Syst. Sci. 23, 2525-2540, https://doi.org/10.5194/hess-23-2525-2019, 2019

Gimeno, L., Stohl, A., Trigo, R.M., Dominguez, F., Yoshimura, K., Yu, L., Drumond, A., Durán-Quesada, A.M., Nieto, R.: Oceanic and terrestrial sources of continental precipitation, Rev. Geophys. 50, RG4003, https://doi.org/10.1029/2012RG000389, 2012

Gimeno, L., Vazquez, M., Eiras-Barca, J., Sori, R., Stojanovic, M., Algarra, I., Nieto, R., Ramos, A.M., Duran-Quesada, A.M., Dominguez, F.: Recent progress on the sources of continental precipitation as revealed by moisture transport analysis, Earth-Sci. Rev. 201, 103070, https://doi.org/10.1016/j.earscirev.2019.103070, 2020

Guo, L., van der Ent, R.J., Klingaman, N.P., Demory, M.-E., Vidale, P.L., Turner, A.G., Stephan, C.C., Chevuturi, A.: Moisture Sources for East Asian Precipitation: Mean Seasonal Cycle and Interannual Variability, J. Hydrometeorol. 20, 657-672, https://doi.org/10.1175/JHM-D-18-0188.1, 2019

Guo, L., van der Ent, R.J., Klingaman, N.P., Demory, M.E., Vidale, P.L., Turner, A.G., Stephan, C.C., Chevuturi, A.: Effects of horizontal resolution and air–sea coupling on simulated moisture source for East Asian precipitation in MetUM GA6/GC2, Geosci. Model Dev. 13, 6011-6028, https://doi.org/10.5194/gmd-13-6011-2020, 2020

Hersbach, H., Bell, B., Berrisford, P., Hirahara, S., Horanyi, A., Munoz-Sabater, J., Nicolas, J., Peubey, C., Radu, R., Schepers, D., Simmons, A., Soci, C., Abdalla, S., Abellan, X., Balsamo, G., Bechtold, P., Biavati, G., Bidlot, J., Bonavita, M., De Chiara, G., Dahlgren, P., Dee, D., Diamantakis, M., Dragani, R., Flemming, J., Forbes, R., Fuentes, M., Geer, A., Haimberger, L., Healy, S., Hogan, R.J., Holm, E., Janiskova, M., Keeley, S., Laloyaux, P., Lopez, P., Lupu, C., Radnoti, G., de Rosnay, P., Rozum, I., Vamborg, F., Villaume, S., Thepaut, J.-N.: The ERA5 global reanalysis, Quart. J. Roy. Meteorol. Soc. 146, 1999-2049, https://doi.org/10.1002/qj.3803, 2020

Hu, Q., Zhao, Y., Huang, A., Ma, P., Ming, J.: Moisture Transport and Sources of the Extreme Precipitation Over Northern and Southern Xinjiang in the Summer Half-Year During 1979–2018, Frontiers in Earth Science 9, https://doi.org/10.3389/feart.2021.770877, 2021

Huang, W., Qiu, T., Yang, Z., Lin, D., Wright, J.S., Wang, B., He, X.: On the formation mechanism for wintertime extreme precipitation events over the southeastern Tibetan Plateau, J. Geophys. Res.-Atmos. 123, 12,692-612,714, https://doi.org/10.1029/2018JD028921, 2018

Keune, J., Schumacher, D.L., Miralles, D.G.: A unified framework to estimate the origins of atmospheric moisture and heat using Lagrangian models, Geosci. Model Dev. 15, 1875-1898, https://doi.org/10.5194/gmd-15-1875-2022, 2022

Li, Y., Su, F., Chen, D., Tang, Q.: Atmospheric Water Transport to the Endorheic Tibetan Plateau and Its Effect on the Hydrological Status in the Region, J. Geophys. Res.-Atmos. 124, 12864-12881, https://doi.org/10.1029/2019jd031297, 2019

Li, Y., Su, F., Tang, Q., Gao, H., Yan, D., Peng, H., Xiao, S.: Contributions of moisture sources to precipitation in the major drainage basins in the Tibetan Plateau, Sci. China-Earth Sci. 65, 1088, https://doi.org/10.1007/s11430-021-9890-6, 2022a

Li, Y., Wang, C., Huang, R., Yan, D., Peng, H., Xiao, S.: Spatial distribution of oceanic moisture contributions to precipitation over the Tibetan Plateau, Hydrol. Earth Syst. Sci. 26, 6413-6426, https://doi.org/10.5194/hess-26-6413-2022, 2022b

Liu, R., Wang, X., Wang, Z.: Atmospheric moisture sources of drought and wet events during 1979–2019 in the Three-River Source Region, Qinghai-Tibetan Plateau, Theor. Appl. Climatol. 149, 487-499, https://doi.org/10.1007/s00704-022-04058-9, 2022

Liu, R., Wen, J., Wang, X., Wang, Z., Liu, Y.: Case studies of atmospheric moisture sources in the source region of the Yellow River from a Lagrangian perspective, Int. J. Climatol. 42, 1516-1530, https://doi.org/10.1002/joc.7317, 2021

Liu, X., Liu, Y., Wang, X., Wu, G.: Large-Scale Dynamics and Moisture Sources of the Precipitation Over the Western Tibetan Plateau in Boreal Winter, J. Geophys. Res.-Atmos. 125, e2019JD032133, https://doi.org/10.1029/2019JD032133, 2020a

Liu, Y., Lu, M., Yang, H., Duan, A., He, B., Yang, S., Wu, G.: Land–atmosphere–ocean coupling associated with the Tibetan Plateau and its climate impacts, Natl. Sci. Rev. 7, 534-552, https://doi.org/10.1093/nsr/nwaa011, 2020b

Ma, Y., Lu, M., Bracken, C., Chen, H.: Spatially coherent clusters of summer precipitation extremes in the Tibetan Plateau: Where is the moisture from?, Atmos. Res. 237, 104841, https://doi.org/10.1016/j.atmosres.2020.104841, 2020

610 Pan, C., Zhu, B., Gao, J., Kang, H., Zhu, T.: Quantitative identification of moisture sources over the Tibetan Plateau and the relationship between thermal forcing and moisture transport, Climate Dyn. 52, 181-196, https://doi.org/10.1007/s00382-018-4130-6, 2018

Pisso, I., Sollum, E., Grythe, H., Kristiansen, N.I., Cassiani, M., Eckhardt, S., Arnold, D., Morton, D., Thompson, R.L., Groot Zwaaftink, C.D., Evangeliou, N., Sodemann, H., Haimberger, L., Henne, S., Brunner, D., Burkhart, J.F., Fouilloux, A.,
615 Brioude, J., Philipp, A., Seibert, P., Stohl, A.: The Lagrangian particle dispersion model FLEXPART version 10.4, Geosci. Model Dev. 12, 4955-4997, https://doi.org/10.5194/gmd-12-4955-2019, 2019

Qiu, T., Huang, W., Wright, J.S., Lin, Y., Lu, P., He, X., Yang, Z., Dong, W., Lu, H., Wang, B.: Moisture Sources for Wintertime Intense Precipitation Events Over the Three Snowy Subregions of the Tibetan Plateau, J. Geophys. Res.-Atmos. 124, 12708-12725, https://doi.org/10.1029/2019jd031110, 2019

620 Shao, L., Tian, L., Cai, Z., Wang, C., Li, Y.: Large-scale atmospheric circulation influences the ice core d-excess record from the central Tibetan Plateau, Climate Dyn. 57, 1805-1816, https://doi.org/10.1007/s00382-021-05779-9, 2021

Sodemann, H., Schwierz, C., Wernli, H.: Interannual variability of Greenland winter precipitation sources: Lagrangian moisture diagnostic and North Atlantic Oscillation influence, J. Geophys. Res.-Atmos. 113, D03107, https://doi.org/10.1029/2007JD008503, 2008

625 Sprenger, M., Wernli, H.: The LAGRANTO Lagrangian analysis tool – version 2.0, Geosci. Model Dev. 8, 2569-2586, https://doi.org/10.5194/gmd-8-2569-2015, 2015

Stein, A.F., Draxler, R.R., Rolph, G.D., Stunder, B.J.B., Cohen, M.D., Ngan, F.: NOAA's HYSPLIT Atmospheric Transport and Dispersion Modeling System, Bull. Amer. Meteorol. Soc. 96, 2059-2078, https://doi.org/10.1175/BAMS-D-14-00110.1, 2016

630 Sun, B., Wang, H.: Moisture sources of semiarid grassland in China using the Lagrangian particle model FLEXPART, J. Climate 27, 2457-2474, https://doi.org/10.1175/JCLI-D-13-00517.1, 2014

Tuinenburg, O.A., Staal, A.: Tracking the global flows of atmospheric moisture and associated uncertainties, Hydrol. Earth Syst. Sci. 24, 2419-2435, https://doi.org/10.5194/hess-24-2419-2020, 2020

van der Ent, R.J., Savenije, H.H., Schaefli, B., Steele-Dunne, S.C.: Origin and fate of atmospheric moisture over continents,
635 Water Resour. Res. 46, W09525, https://doi.org/10.1029/2010WR009127, 2010

van der Ent, R.J., Tuinenburg, O.A., Knoche, H.R., Kunstmann, H., Savenije, H.H.G.: Should we use a simple or complex model for moisture recycling and atmospheric moisture tracking?, Hydrol. Earth Syst. Sci. 17, 4869-4884, https://doi.org/10.5194/hess-17-4869-2013, 2013

van der Ent, R.J., Wang-Erlandsson, L., Keys, P.W., Savenije, H.H.G.: Contrasting roles of interception and transpiration in
640 the hydrological cycle – Part 2: Moisture recycling, Earth Syst. Dynam. 5, 471-489, https://doi.org/10.5194/esd-5-471-2014, 2014

Wang, L., Liu, W., Xu, Z., Zhang, J.: Water sources and recharge mechanisms of the Yarlung Zangbo River in the Tibetan Plateau: Constraints from hydrogen and oxygen stable isotopes, J. Hydrol. 614, 128585, https://doi.org/10.1016/j.jhydrol.2022.128585, 2022

645 Wang, Y., Yang, K., Huang, W., Qiu, T., Wang, B.: Dominant Contribution of South Asia Monsoon to External Moisture for Extreme Precipitation Events in Northern Tibetan Plateau, Remote Sensing 15, 735, https://doi.org/10.3390/rs15030735, 2023

Winschall, A., Pfahl, S., Sodemann, H., Wernli, H.: Comparison of Eulerian and Lagrangian moisture source diagnostics – the flood event in eastern Europe in May 2010, Atmos. Chem. Phys. 14, 6605-6619, https://doi.org/10.5194/acp-650 14-6605-2014, 2014

Xu, Y., Gao, Y.: Quantification of Evaporative Sources of Precipitation and Its Changes in the Southeastern Tibetan Plateau and Middle Yangtze River Basin, Atmosphere 10, 428, https://doi.org/10.3390/atmos10080428, 2019

Yang, K., Wu, H., Qin, J., Lin, C., Tang, W., Chen, Y.: Recent climate changes over the Tibetan Plateau and their impacts on energy and water cycle: A review, Glob. Planet. Change 112, 79-91, https://doi.org/10.1016/j.gloplacha.2013.12.001, 2014

655 Yang, S., Zhang, W., Chen, B., Xu, X., Zhao, R.: Remote moisture sources for 6-hour summer precipitation over the Southeastern Tibetan Plateau and its effects on precipitation intensity, Atmos. Res. 236, 104803, https://doi.org/10.1016/j.atmosres.2019.104803, 2020

Yao, S., Jiang, D., Zhang, Z.: Lagrangian simulations of moisture sources for Chinese Xinjiang precipitation during 1979–2018, Int. J. Climatol. 41, E216-E232, https://doi.org/10.1002/joc.6679, 2020

660    Yao, S., Jiang, D., Zhang, Z.: Moisture Sources of Heavy Precipitation in Xinjiang Characterized by Meteorological Patterns, J. Hydrometeorol. 22, 2213-2225, https://doi.org/10.1175/JHM-D-20-0236.1, 2021

Yao, T., Bolch, T., Chen, D., Gao, J., Immerzeel, W., Piao, S., Su, F., Thompson, L., Wada, Y., Wang, L., Wang, T., Wu, G., Xu, B., Yang, W., Zhang, G., Zhao, P.: The imbalance of the Asian water tower, Nature Reviews Earth & Environment https://doi.org/10.1038/s43017-022-00299-4, 2022

665    Yao, T., Masson-Delmotte, V., Gao, J., Yu, W., Yang, X., Risi, C., Sturm, C., Werner, M., Zhao, H., He, Y.: A review of climatic controls on δ18O in precipitation over the Tibetan Plateau: Observations and simulations, Rev. Geophys. 51, 525-548, https://doi.org/10.1002/rog.20023, 2013

Yao, T., Xue, Y., Chen, D., Chen, F., Thompson, L., Cui, P., Koike, T., Lau, W.K.-M., Lettenmaier, D., Mosbrugger, V.: Recent Third Pole's rapid warming accompanies cryospheric melt and water cycle intensification and interactions between
670    monsoon and environment: multi-disciplinary approach with observation, modeling and analysis, Bull. Amer. Meteorol. Soc. 100, 423-444, https://doi.org/10.1175/BAMS-D-17-0057.1, 2018

Zhang, C.: Moisture source assessment and the varying characteristics for the Tibetan Plateau precipitation using TRMM, Environ. Res. Lett. 15, 104003, https://doi.org/10.1088/1748-9326/abac78, 2020

Zhang, C., Chen, D., Tang, Q., Huang, J.: Fate and Changes in Moisture Evaporated From the Tibetan Plateau (2000–2020),
675    Water Resour. Res. 59, e2022WR034165, https://doi.org/10.1029/2022WR034165, 2023a

Zhang, C., Tang, Q., Chen, D.: Recent changes in the moisture source of precipitation over the Tibetan Plateau, J. Climate 30, 1807-1819, https://doi.org/10.1175/JCLI-D-15-0842.1, 2017

Zhang, C., Tang, Q.H., Chen, D.L., van der Ent, R.J., Liu, X.C., Li, W.H., Haile, G.G.: Moisture Source Changes Contributed to Different Precipitation Changes over the Northern and Southern Tibetan Plateau, J. Hydrometeorol. 20, 217-229,
680    https://doi.org/10.1175/Jhm-D-18-0094.1, 2019a

Zhang, C., Zhang, X., Tang, Q., Chen, D., Huang, J., Wu, S., Liu, Y.: Quantifying precipitation moisture contributed by different atmospheric circulations across the Tibetan Plateau, J. Hydrol. 628, 130517, https://doi.org/10.1016/j.jhydrol.2023.130517, 2024

Zhang, Q., Shen, Z., Pokhrel, Y., Farinotti, D., Singh, V.P., Xu, C., Wu, W., Wang, G.: Oceanic climate changes threaten the
685    sustainability of Asia's water tower, Nature 615, 87-93, https://doi.org/10.1038/s41586-022-05643-8, 2023b

Zhang, Y., Huang, W., Zhong, D.: Major Moisture Pathways and Their Importance to Rainy Season Precipitation over the Sanjiangyuan Region of the Tibetan Plateau, J. Climate 32, 6837-6857, https://doi.org/10.1175/jcli-d-19-0196.1, 2019b

Zhao, R., Chen, B., Xu, X.: Intensified Moisture Sources of Heavy Precipitation Events Contributed to Interannual Trend in Precipitation Over the Three-Rivers-Headwater Region in China, Frontiers in Earth Science 9,
690    https://doi.org/10.3389/feart.2021.674037, 2021

Zhao, R., Chen, B., Zhang, W., Yang, S., Xu, X.: Moisture source anomalies connected to flood-drought changes over the three-rivers headwater region of Tibetan Plateau, Int. J. Climatol. 43, 5303-5316, https://doi.org/10.1002/joc.8147, 2023

Zhou, Y., Xie, Z., Liu, X.: An Analysis of Moisture Sources of Torrential Rainfall Events over Xinjiang, China, J. Hydrometeor. 20, 2109-2122, https://doi.org/10.1175/JHM-D-19-0010.1, 2019

695